Tectonophysics 891 (2024) 230527

Contents lists available at ScienceDirect

Tectonophysics

journal homepage: www.elsevier.com/locate/tecto

Morphostructural evidence of crustal-scale, active along-strike segmentation of the Umbria-Marche Apennines, Italy

S. Teloni [a], E. Valente [b,*], A. Ascione [b], S. Mazzoli [a], P.P. Pierantoni [a], M.C. Invernizzi [a]

[a] School of Science and Technology – Geology Division, University of Camerino, Via Gentile III da Varano, 62032 Camerino, MC, Italy
[b] Department of Earth, Environment and Resources Sciences - DiSTAR, University of Naples Federico II, Complesso Universitario Monte Sant'Angelo, via Vicinale Cupa Cintia 21, 80126 Naples, Italy

ARTICLE INFO

Keywords:
Swath profile
Chi-plot
Normalized steepness index
Differential uplift
Apennines

ABSTRACT

This paper discusses the response of topography and river networks to non-uniform lithology and tectonic forcing in the Umbria-Marche sector of the Apennines fold and thrust belt. We ruled out the role of variable erosion of rock types and interpret channel steepness data in terms of rock uplift, discovering a southward increase in the total amount of uplift. Such a trend appears as the large-scale response to uneven vertical motions of different sectors of the mountain ridge and foothills. The general coincidence between sector boundaries and transversal, NE-SW striking faults mapped by seismic interpretation in the outer zone of the fold and thrust belt, suggests that such faults extend to the SW, beneath the allochthonous thrust sheets of the mountainous area. Therefore, it may be inferred that such transversal faults represent long-lived, deeply rooted basement structures compartmentalizing both the axial and the outer zones of the fold and thrust belt. We suggest that differential uplift was essentially controlled by variable amounts of basement thrust displacement characterizing the compartmentalized belt. This interpretation deviates from a more conventional view that uplift of the central Apennines, particularly prominent in the south, is dynamically supported. Our results, besides shedding new light into the active tectonic behavior of a large portion of the Italian peninsula, also provide general insights into the surface response to the differential behavior of crustal blocks produced by along-strike segmentation of active mountain belts.

1. Introduction

Morphotectonic studies are focused on unraveling the topographic and river network signature of vertical motion distribution (Bishop, 2007; Bull, 2008; Bull and McFadden, 1977; Burbank and Anderson, 2011). The morphotectonic approach has been adopted in different tectonic settings of the world (e.g., Di Biase et al., 2010; Keller and Pinter, 2002; Lanari et al., 2022; Obaid and Allen, 2019; Schildgen et al., 2012; Scotti et al., 2014). The recent development of several GIS and MATLAB based analyses on digital elevation models (Jaiswara et al., 2020; Schwanghart and Kuhn, 2010; Schwanghart and Scherler, 2014; Whipple et al., 2007) has strongly contributed to the large diffusion of morphotectonic analysis at the orogen scale. Several indicators and parameters, such as swath profiles, Ksn index, river long profile and chi plots, have been used to infer the spatial distribution of surface motion in mountain belts (Basilici et al., 2020; Eizenhöfer et al., 2019; Forte et al., 2014; Gallen and Wegmann, 2017; Racano et al., 2021; Pazzaglia and Fisher, 2022). Quantitative analyses of the topography and river network have been applied to the reconstruction of the orogenic growth of the Apennines (e.g., Ascione et al., 2008; Calderoni et al., 2010; D'Agostino et al., 2001; D'Alessandro et al., 2003; Delchiaro et al., 2024; Della Seta et al., 2008; Ferrarini et al., 2021; Lanari et al., 2023; Mayer et al., 2003; Miccadei et al., 2017; Pazzaglia and Fisher, 2022; Piacentini and Miccadei, 2014; Racano et al., 2020; Sembroni et al., 2020; Vannoli et al., 2004). Among the main findings of these works is the identification of an uneven uplift along the strike of the mountain range. Multiple datasets and observations point out that the central Apennines are uplifting faster than the northern sectors of the belt, at least since Quaternary times. These datasets include stable isotopes (San Jose et al. (2020), U-Th-He cooling ages (Fellin et al., 2022), geophysical and geodetic datasets (Faccenna et al., 2014; Serpelloni et al., 2013) and linear inversion of river long profiles (Pazzaglia and Fisher, 2022; Racano et al., 2024). The uneven uplift in the Apennines is related to deep processes (e.g., Lanari et al., 2023; Racano et al., 2024). This

* Corresponding author.
E-mail address: ettore.valente@unina.it (E. Valente).

https://doi.org/10.1016/j.tecto.2024.230527
Received 29 January 2024; Received in revised form 20 September 2024; Accepted 5 October 2024
Available online 9 October 2024

suggests that the topography of the Apennines is dynamically sustained, thus implying a major role of deep (i.e., mantle-related) geodynamic processes (D'Agostino et al., 2001; Faccenna et al., 2014; Fellin et al., 2022). In this study, we challenge the idea that large-scale geodynamics is driving non-uniform uplift in the Apennines and suggest that lithospheric, rather than sub-lithospheric mantle processes, are dominant in this active plate boundary setting.

With the aim of obtaining further constraints on the pattern of the long-term uplift of the central Apennines, we performed a large-scale morphotectonic analysis of the topography and river network features of the Adriatic slope of the Umbria-Marche Apennines. The Umbria-Marche Apennines and Foothills (UMAF) are characterized by a marked lithological variability and an almost systematic association of carbonate rocks and arenaceous-marly-clayey deposits with the main ridges and topographic lows, respectively. Bearing in mind that the recognition of active tectonic perturbations rests on the identification of the control exerted by lithology on the parameters of topography and drainage network (e.g., Bernard et al., 2019; Clementucci et al., 2022; Pazzaglia et al., 1998; Seagren and Schoenbohm, 2019; Stock and Montgomery, 1999), we compared the results of our morphotectonic analysis with the spatial distribution of outcropping rock types and tectonic structures. The comparison allowed us to define the extent to which the lithological inhomogeneity affects the morphometric parameters of the drainage network. The resulting, unmasked tectonic signal reveals much of the pattern of the large scale along-strike variability of vertical motions. This, in turn, may have implications on seismicity distribution, thus providing new insights into the active tectonic behavior of a large sector of the Italian peninsula.

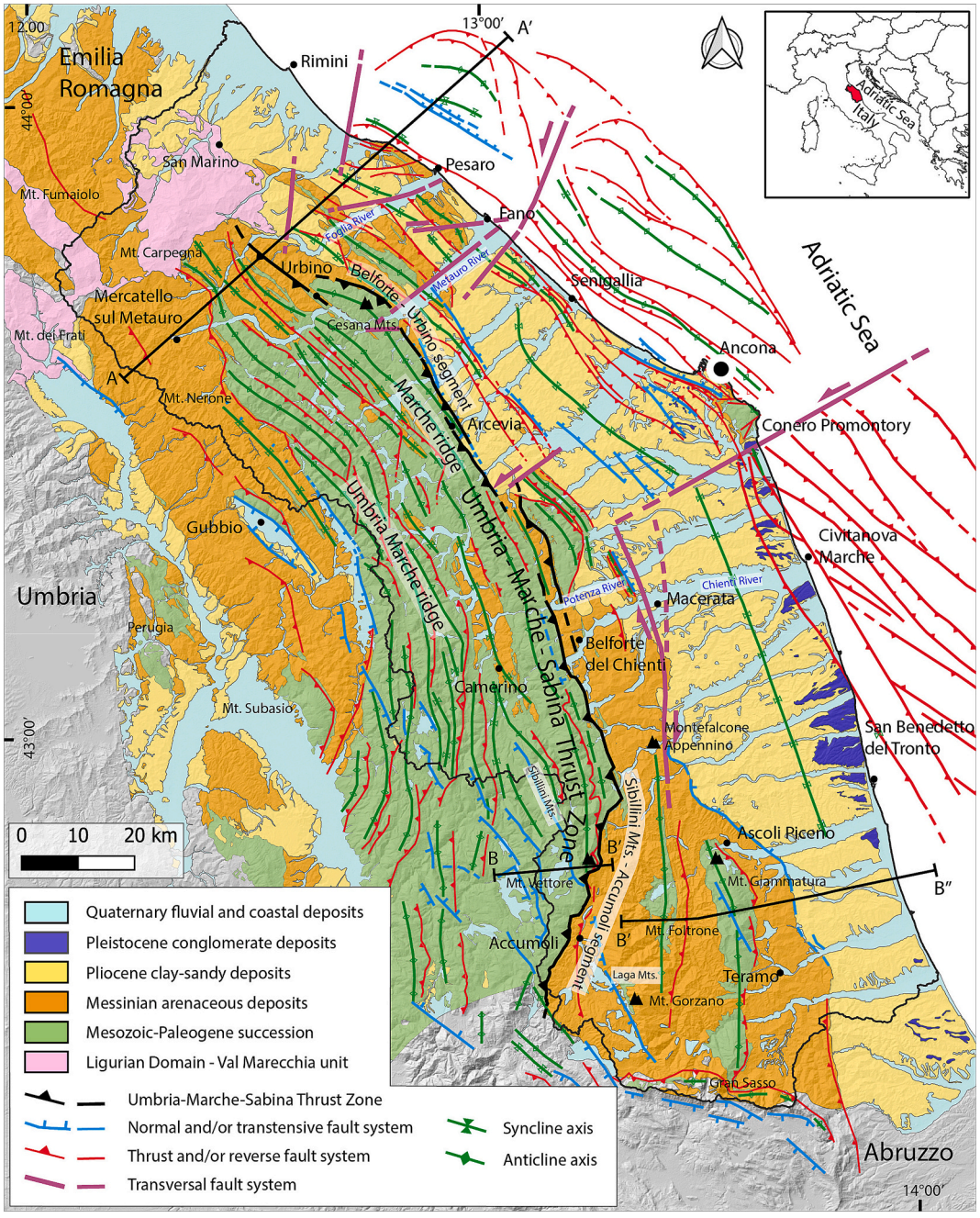

Fig. 1. Structural map of the UMAF and offshore area (modified from Costa et al., 2021 and Pierantoni et al., 2019). Cross-section traces of Fig. 2 are shown (A-A', B-B' and B'-B″ segments).

2. Tectonic framework of the study area

The study area is located in the central–eastern sector of the Italian peninsula (Fig. 1), within the UMAF, which forms part of the peri-Mediterranean Alpine orogenic belt. The Apennines are an arcuate, mostly NW-SE striking fold and thrust belt (Calamita et al., 1994), which evolved during the Neogene in the frame of Africa-Eurasia plate convergence since the Late Cretaceous (Dewey et al., 1989; Mazzoli and Helman, 1994; Turco et al., 2021). Since the Late Miocene, back-arc extension in the hinterland (Tyrrhenian Sea) was coeval with thrusting in the frontal part of the belt (e.g., Butler et al., 2004). Therefore, the Apennines represent a mountain belt characterized by diverse, active geodynamic processes. Defining the relative importance of dynamic (circulating sub-lithospheric, ductile mantle) and tectonic (lithospheric) processes to the building of topography may be difficult (Faccenna et al., 2014). Extension and crustal thinning in the western side of the orogen are well established, as are tectonic accretion and crustal thickening in the eastern side (Butler et al., 2004). However, variable uplift rates and building of topography along the strike of the mountain belt appear to be associated with differential vertical motion of crustal blocks bounded by transversal faults (Calamita et al., 1994; Calamita and Pizzi, 1994). These, in turn, could be variably related with deeper geodynamic processes such as the lateral and vertical propagation of lithospheric tears, slab segmentation and break-off (Ascione et al., 2012; Cinque et al., 1993; Lucente et al., 1999; Mele et al., 1998; Montuori et al., 2007; Spakman, 1990; Spakman and Wortel, 2004; Westaway, 1993; Wortel and Spakman, 2000; Piromallo and Morelli, 2003).

2.1. Geological and morphostructural setting

The tectonic evolution of the study area consists of three main stages:

(1) Pre-orogenic stage (Trias-Paleogene): the Adria rifted continental margin hosted a carbonate platform that was dissected by faulting during the second part of the Early Jurassic, leading to the development of a series of horsts and grabens/half grabens accompanied by transversal oblique-slip transfer faults segmenting the extensional system (Centamore et al., 2002; Centamore and Rossi, 2009; Mazzoli et al., 2005; Pierantoni et al., 2013; Scisciani et al., 2014). Rifting followed by thermal subsidence allowed the deposition of the well-bedded, calcareous-

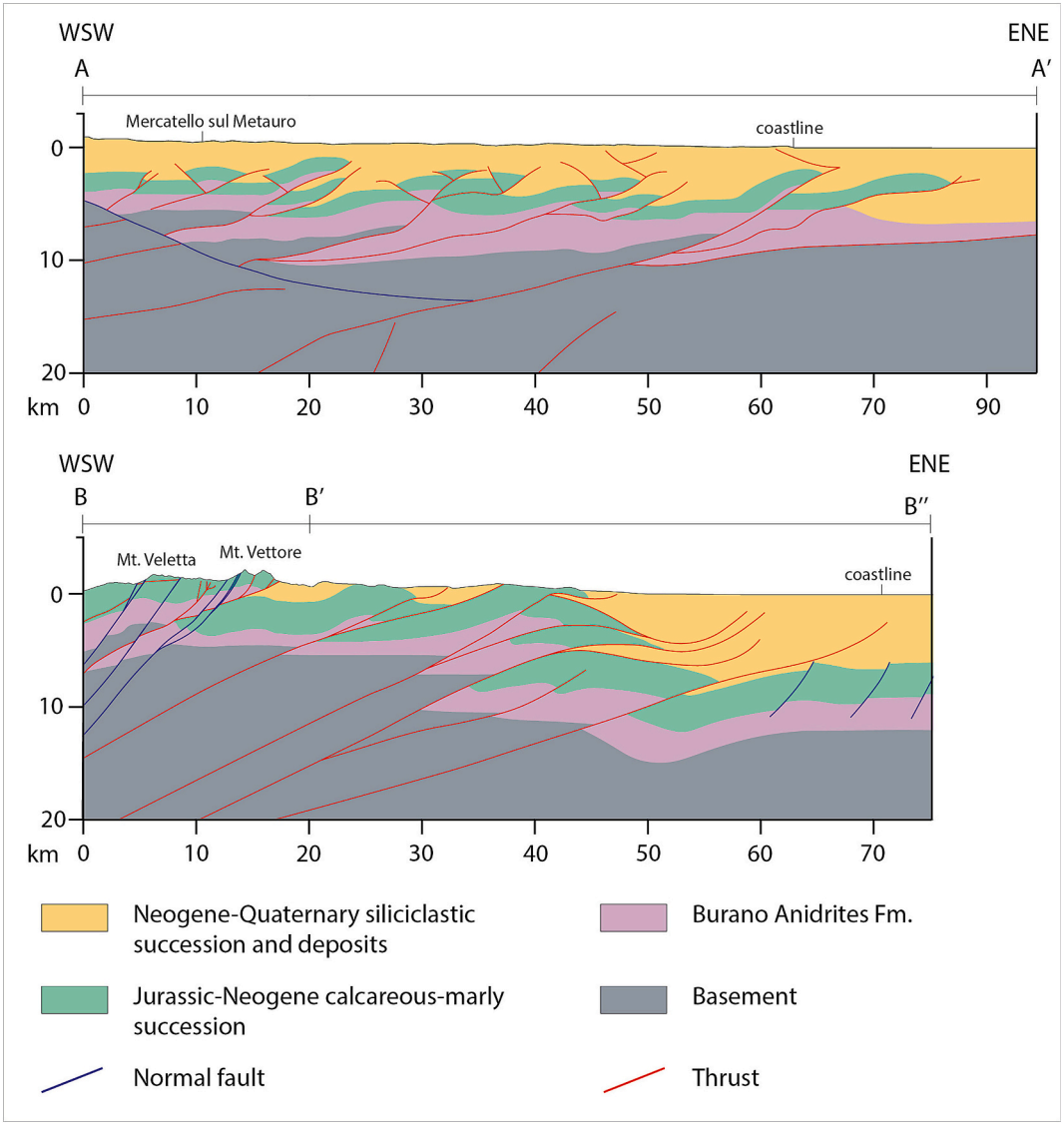

Fig. 2. Regional geological sections across the UMAF. Northern section (A-A') modified after Santini et al., 2016. The composite southern section includes segments B-B' (modified after Barchi et al., 1998) and B'-B″ (modified after Pace et al., 2015). Section traces are in Fig. 1.

marly Umbria-Marche sedimentary succession (Centamore et al., 2002).

(2) Syn-orogenic stage (Miocene-Pliocene): the various sectors of the study area were progressively involved in the fold and thrust belt from west to east, as shown by synorogenic siliciclastic deposits filling a migrating foreland basin system (Centamore et al., 2002). The basement is also involved in the thrust system (e.g., Coward et al., 1999). Transversal faults (probably inherited from the pre-orogenic stage) also controlled differential shortening in adjacent crustal sectors (Calamita et al., 1994; Calamita and Pizzi, 1994).

(3) Late-orogenic stage: a general eastward migration of the thrust front towards the foreland characterized the Pliocene to present time (Barchi et al., 2012; Patacca et al., 1990). The hinterland and then the axial zone of the Umbria-Marche Apennines were affected by extension generating NW-SE-striking crustal normal faults (Barchi and Mirabella, 2009; Dewey, 1988; Doglioni, 1995; Keller et al., 1994). Extensional basins host continental deposits (e.g. Gubbio, Norcia and Colfiorito basins; Brogi et al., 2014; Cipollari et al., 1999; Cosentino et al., 2017; Doglioni et al., 1998; Galadini and Messina, 2001; Mancini et al., 2005; Martini and Sagri, 1993), while active thrusts in the Adriatic offshore are buried by thick Pliocene-Quaternary foreland basin deposits (e.g., Santini et al., 2021; Fig. 2) whose sedimentation rate largely exceeds thrust slip rates (e.g., Basili and Barba, 2007; Pezzo et al., 2023).

The western (i.e., inner) sector of the UMAF includes two anticlinal ridges known as the Umbria-Marche ridge (UMR) and the Marche ridge (MR) (Fig. 1). These ridges expose the Mesozoic-Paleogene Umbria-Marche succession (a calcareous and marly succession with thickness ranging between 1000 and 2000 m) at elevations locally exceeding 2000 m. The intervening valley is a broad synclinorium cored by Upper Miocene terrigenous deposits (Fig. 1). In the eastern (i.e., outer) sector of the UMAF, folds and thrusts exposed at the surface involve mainly the Messinian siliciclastic succession (ranging in thickness from a few hundred meters to the north to 3000 m to the south) and marine to continental Plio-Pleistocene terrigenous deposits of the Marche foothills (Fig. 2).

Located along the eastern edge of the MR, the Apennines Mountain front is bounded eastward by the Umbria-Marche-Sabina Thrust Zone (UMSTZ; Fig. 1). The UMSTZ is a major thrust fault consisting of several WNW-ESE to NE-SW striking, right-stepping en-échelon segments. Generally, the UMSTZ is composed of two main thrust portions with an overlap zone 10 to 20 km wide between the Potenza River and the Chienti River valleys (Fig. 1). The northern, Belforte-Urbino thrust segment has a general NW-SE trend, changing to WNW-ESE north of the Metauro River valley (Fig. 1). The Belforte-Urbino thrust is imaged in two seismic profiles (including the CROP03 deep seismic reflection profile; Barchi et al., 1998; Calamita et al., 1991). It shows offsets ranging from 2 km to 4.5 km (Mazzoli et al., 2005). The latest thrust activity in this section is attributable to the late Messinian (Deiana et al., 2003). The southern, Sibillini Mts. - Accumoli segment (Fig. 1) experienced the maximum horizontal displacements along the UMSTZ, with values of about 10 km (Mazzoli et al., 2005; Fig. 2). This thrust controlled the mountain front during the Messinian deposition of the Laga Fm. The late stages of activity of this thrust occurred during post-evaporitic late Messinian time, with local slip continuing into the Pliocene (Mazzoli et al., 2005, and references therein).

The foothills and coastal areas are traversed by nearly equally-space transverse rivers with headwaters that are subsequent to structure. The river network consists of NE-SW oriented, NE flowing main trunks and related tributaries, flowing within a couple of kilometers to tens kilometers spaced transverse valleys. Most of the NE-SW trending rivers cut the anticline carbonate ridges forming very deeply incised gorges, and locally follow the syncline structures (e.g., the upper Esino River valley) for several kilometers. The long-term evolution of the river network was characterized by superimposition and stream-piracy phenomena in the axial zone of the fold-and-thrust belt, and in the formation of a staircase of strath and fill terraces in the outer zone (i.e., the foothills; Mayer et al., 2003; Nesci et al., 2012; Wegmann and Pazzaglia, 2009). Valley evolution in the foothills followed the mechanism of diverging drainage initially formed on either the top depositional surface of fans or the correlative erosional glacis, whose cone-shaped morphology caused the divergence from the primitive channel (Nesci and Savelli, 2003). Quaternary normal faults are well known to exert a major control on the topography of the study area, particularly in the southern part of the region (e.g., Gentili et al., 2017). Indeed, Della Seta et al. (2008) has highlighted the role of tectonics in shaping the landscape, as several structurally controlled landforms (e.g., rectilinear ridges and valleys, fluvial capture, beheaded valleys, faceted spurs) and offset alluvial terraces suggest a Late Pleistocene activity of NW-SE, WNW-ESE and NE-SW striking fault segments.

2.2. Seismicity

The UMAF are the locus of moderate to intense tectonic activity, as shown by (i) instrumental baseline seismicity, (ii) the occurrence of several historical strong earthquakes (e.g. the Mw 6.92, 1703 Valnerina earthquake, which formed part of a 3-earthquakes sequence that struck the whole central Italy; the Mw 6.17, 1741 Fabriano earthquake; the Mw 6.51, 1781 Cagli earthquake and the Mw 6.18, 1799 Camerino earthquake - Castelli and Monachesi, 2001; Monachesi et al., 1991; Rovida et al., 2022; Stucchi et al., 1991), and (iii) recent seismic sequences (e.g. the 1997–1998 Colfiorito seismic sequence with Mw 6.0 main shock - Chiaraluce et al., 2004; the 2016–2017 Amatrice-Visso-Norcia seismic sequence with maximum magnitude 6.5 - Civico et al., 2018; EMERGEO Working Group, 2016). Some of these earthquakes, including the recent Amatrice-Visso-Norcia seismic sequence, are clearly linked to normal faults in the topographic axis of the chain while others, like the Cagli earthquake or Fabriano earthquake that are located further east, are not associated with any clear emergent fault.

The seismicity of the Marche foothills and Adriatic offshore is characterized by moderate historical events. The seismotectonic behavior of this sector is consistent with the activity of a highly segmented thrust system (Coward et al., 1999) dominantly including NW-SE striking thrust faults and WSW-ENE striking strike-slip faults (e.g., Basili and Barba, 2007; Costa et al., 2021; Mazzoli et al., 2014; Vannoli et al., 2015; Fig. 3).

3. Material and methods

A GIS-aided analysis of both topography and river network has been carried out to unravel vertical motion distribution within the UMAF. The 30 m NASA ASTER GDEM V2 (https://asterweb.jpl.nasa.gov/gdem.asp, last access on 8 December 2022) provided the dataset for morphotectonic analysis through ArcGis 10.8 © and Matlab © software. To compare the results of the morphotectonic analysis with the lithological and active tectonics framework of the UMAF, we constructed a lithological map of the study area and analyzed seismicity distribution using all available instrumental seismic data.

3.1. Topography analysis

Topography is quantified using topographic envelope and sub-envelope maps, which have been coupled with the analysis of seven swath profiles. The spatial distribution of elevation depends on both the resistance to erosion of the outcropping rocks and tectonics (e.g., surface uplift). The maximum elevation mainly reflects the spatial distribution of rock-types, while mean elevation is representative of surface uplift distribution (England and Molnar, 1990) and minimum elevation reflects valley floor distribution (Valente et al., 2019). In addition, spatial

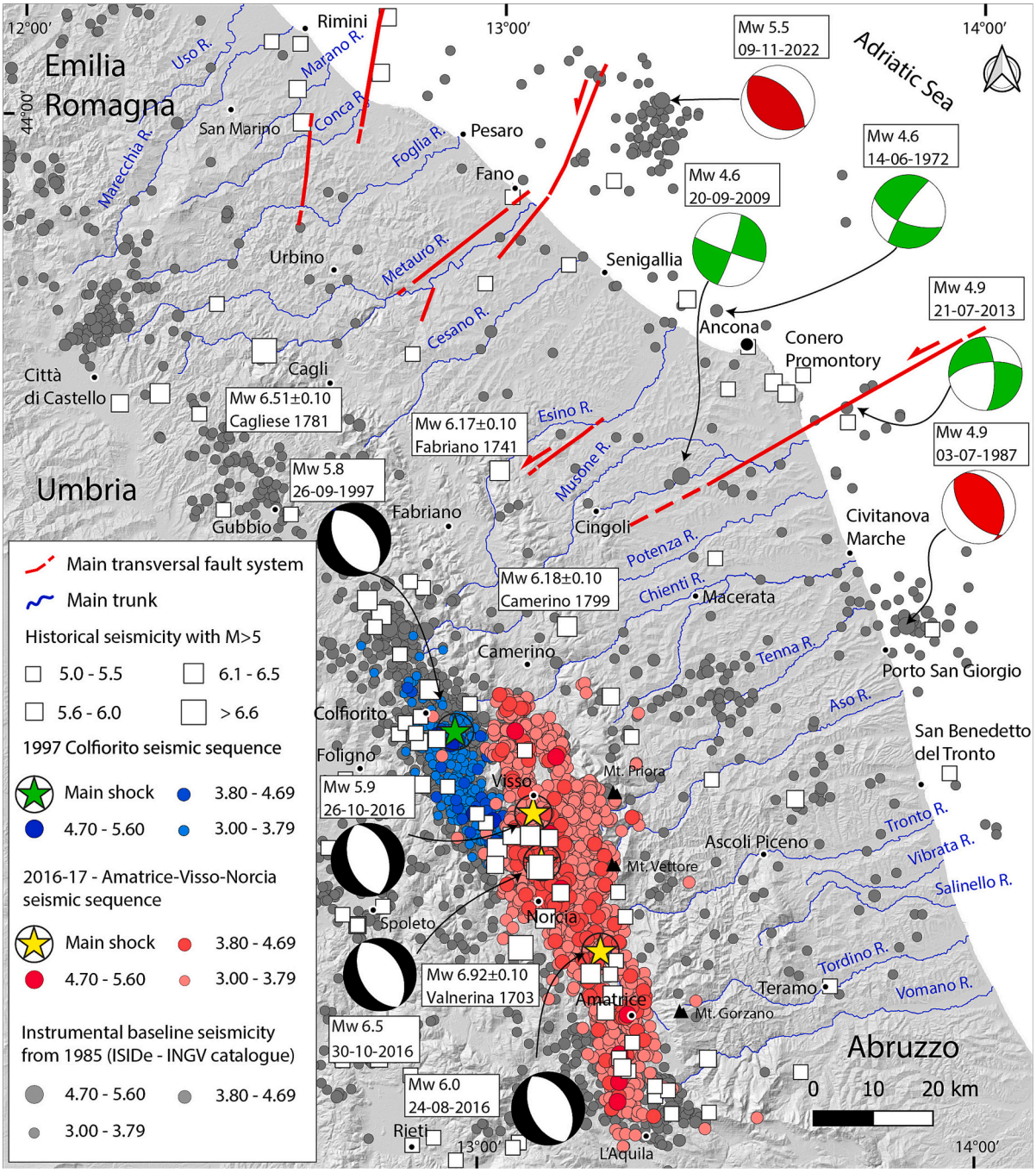

Fig. 3. Historical (white boxes) and instrumental seismicity with magnitude higher than 3 (circles) for the eastern central Italy and surrounding area. Red circles show the 2016–2017 Amatrice-Visso-Norcia seismic sequence whereas yellow stars highlight the main shocks. Blue circles and green stars represent the 1997 Colfiorito seismic sequence and main shock (Mw 5.8) respectively. Gray circles show other seismic events included in the ISIDe database. Focal mechanism solutions (black: dominant normal faulting; green: dominant strike-slip faulting; red: dominant reverse faulting) are from ISIDe database (ISIDe Working Group, 2007) and from Mazzoli et al. (2014) and Santini et al. (2011). White squares represent historical seismic events with M > 5 (Rovida et al., 2022). (For interpretation of the references to colour in this figure legend, the reader is referred to the web version of this article.)

variations in uplift may be revealed by local relief distribution, especially in areas where rock types with homogeneous resistance to erosion outcrop (Di Biase et al., 2010). Maximum, mean and minimum elevation maps have been derived by applying a 5 × 5 km large moving window to the 30 m DTM, whereas relief map has been derived as the difference between maximum and minimum elevation.

Swath profiles analysis has been carried out using the SwathProfiler ArcGIS add-in tool (Pérez-Peña et al., 2017). Seven swath profiles, 20 km in width and with different orientations were constructed: five profiles, with SW-NE orientations, are roughly perpendicular to the trend of the UMAF; one profile follows the bending of the UMAF arc, thus including both chain and foreland units; one profile, NW-SE trending, moves within the foothills underlain by foredeep units.

3.2. Analysis of the river network

River network analysis included the construction of river longitudinal profiles and transformed river long profiles (chi-plot), which have

been coupled with the slope/area analysis to derive the spatial distribution of the normalized channel steepness index (Ksn). Analyzed rivers are 18 main trunks that drain from the SW to the NE across the UMAF.

We analyzed the river network by means of the Topotoolbox scripts of Matlab (Schwanghart and Kuhn, 2010; Schwanghart and Scherler, 2014) and the Run-Chi profiler script (Gallen and Wegmann, 2017). Slope/area analysis relates channel slope with the drainage area following the equation:

$$S = k_s A^{-\theta} \quad (1)$$

where S is the channel slope, ks is the steepness index, A is the drainage area and θ is the concavity index. The analysis is synthesized in a log-log slope vs area diagram with θ being the angle of the regression line and the ks being the y-intercept. Because small variation in θ may provide significant variation in the y-intercept, to compare basins with different drainage areas a reference concavity must be defined. We determined a reference concavity (θ_{ref}) of 0.59 that derives from averaging concavity values between each of the 18 analyzed drainage basins. Furthermore, a smoothing window of 500 m and a reference drainage area $A_0 = 1\ km^2$ have been adopted. The resulting steepness index is named Ksn (normalized steepness index).

The dependence of the Ksn index from bedrock lithology is well established in various climatic environments (e.g., Bernard et al., 2019; Das et al., 2022; Fadul et al., 2022). We evaluated such dependency by means of a statistical analysis of the Ksn values as a function of lithology and presented the results as a box and whisker plot. The lithological control on parameters of topography and river network may be quantified by defining erodibility value (K) of eq. 2. Assuming a simple stream power model where $n = 1$, the Ksn values could be converted to erodibility values (K) using K = E/Ksn. This analysis would require compiling all available erosion rate data for the study area (Pazzaglia and Fisher, 2022).

Bedrock variability at the drainage basin scale may also control the formation of convex upward reaches in the long profiles named knickpoint. These have been classified according to their proximity to contacts between different rock types following the method proposed by Buscher et al. (2017): knickpoints that are less than 200 m far from lithological contacts have been classified as "lithology-controlled knickpoints", whereas knickpoints that are more than 200 m far from lithological contact have been classified as "non-lithology-controlled knickpoints".

Further information about the rivers' response to external perturbations (i.e., tectonics) may be revealed by transformed river long profiles (Perron and Royden, 2013; Royden and Perron, 2013). Transformed river long profiles dissecting a uniform rock-type and equilibrated with uplift have a linear shape, with ks being the slope of the transformed profiles. To obtain transformed river long profiles (chi plots), Eq. 1 can be rewritten as follows:

$$S = \left(\frac{U}{K}\right)^{\frac{1}{n}} A^{-\frac{m}{n}} \quad (2)$$

where U is the rock uplift rate, K is an erodibility coefficient, A is the drainage area, and m and n are constants. Under constant U and K, separating variables in Eq. 2 and integrating them, produces

$$z(x) = z(x_b) + \left(\frac{U}{K A_0^m}\right)^{\frac{1}{n}} \chi \quad (3)$$

with

$$\chi = \int_{x_b}^{x} \left(\frac{A_0}{A(x)}\right)^{\frac{m}{n}} dx \quad (4)$$

where z(x) is the elevation of an observation point along the river long profile, $z(x_b)$ is the elevation of the local base level, A(x) is the drainage area at the observation point z(x), A_0 is a reference drainage area, and m/n is the reference concavity. We set the reference drainage area (A_0) to 1 km^2 whereas the smoothing window is 500 m.

In the chi-plot analysis it is crucial the recognition of the best-fit m/n ratio (θ, reference concavity) at the drainage basin scale, whereas to compare rivers with different drainage areas a reference concavity must be defined, which derives from averaging the m/n values of all the analyzed rivers (Perron and Royden, 2013). The best fit m/n ratio at the basin scale has been derived by the Bayesian optimization script of Topotoolbox (Schwanghart and Kuhn, 2010; Schwanghart and Scherler, 2014). To compare chi-plots among the 18 investigated rivers we derived an average reference concavity value of 0.59.

4. Results

4.1. Distribution of seismicity in the UMAF

The instrumental seismic data recorded since 1985 from the Italian Seismological Instrumental and Parametric Data-Base (http://terremoti.ingv.it/iside ISIDe -INGV, last access on 24 January 2023) and the relocalized earthquakes by INGV Ancona (Cattaneo et al., 2017) have been downloaded and merged together in a new database to analyze seismicity distribution. In this regard, a dataset of 4016 earthquakes data have been selected among more than 70.000 events upon the horizontal error (erh < 2.5 km), vertical error (erz < 2.5 km) and number of phases of the seismogram (> 8), which are considered reliable to avoid uncertainties due to epicenters position. In this dataset the 2016–2017 Amatrice-Visso-Norcia seismic sequence and the 1997 Colfiorito seismic sequence are also present and differentiated from the baseline seismicity (Fig. 3) through the ZMAP decluster algorithm (Wiemer, 2001).

The map of Fig. 3 shows that earthquakes are mainly clustered in the SW sector of the UMAF (i.e., the Sibillini Mts.), which was struck by the 2016–2017 Amatrice-Visso-Norcia seismic sequence. Both the location of the major historical earthquakes and the spatial distribution of instrumental seismicity confirm the intense tectonic activity along the UMR and the MR. Here, the highest magnitude concentrated in the southern sector, as highlighted by the 2016–2017 seismic sequence. Seismic events with magnitude ranging between 3 and 6.5 are generally located along the chain axis and associated with NW-SE striking normal faults, including the Monte Vettore and Monte Gorzano faults. The 2016–2017 aftershocks are confined between the Chienti River valley to the north and the Vomano River valley to the south. Earthquake focal mechanism solutions available from the ISIDe database (ISIDe Working Group, 2007) indicate a predominant normal faulting along the Apennines (Fig. 3), with NE-SW oriented T-axis in agreement with the Quaternary tectonics of this sector (Frepoli and Amato, 1997).

The Marche foothills and Adriatic offshore are characterized by moderate historical events and low to moderate instrumental seismicity (e.g., Mw 5.83, 1930 Senigallia earthquake, Mw 4.68, 1972 Ancona earthquake, Mw 4.90, 1987 Porto San Giorgio earthquake, Mw 4.00, 2022 Costa Marchigiana-Picena earthquake; ISIDe Working Group, 2007; Monachesi et al., 1991; Rovida et al., 2022). Earthquake focal mechanism solutions include NW-SE striking thrust faulting and WSW-ENE oriented strike-slip faulting (e.g., Basili and Barba, 2007; Costa et al., 2021; Costa et al., 2023; Mazzoli et al., 2014; Vannoli et al., 2004, 2015; Fig. 3).

4.2. Lithological map of the UMAF

Detecting the lithological signature on topography and drainage network metrics is crucial to avoid errors in interpreting the spatial distribution of these parameters as due only to tectonics. For this reason, we modified the 1:250.000 geologic map of the northern Apennines (Conti et al., 2020), and lithostratigraphic units have been grouped in eleven categories according to their lithology and stratigraphical position. The derived simplified geological map (Fig. 4) has been used as a

Fig. 4. Geological sketch of UMAF (modified from Conti et al., 2020). The geologic units were grouped into 11 rock categories according to their lithology and stratigraphical position. Dotted black line limits the high Ksn value area of Fig. 11 (see Section 4.4).

reference frame for interpreting the results of topography and river network analyses.

In the northernmost sector of the UMAF, highly allochthonous tectonic units belongto the Ligurian domain. These units are represented by the Val Marecchia 'chaotic' units (unit 11 in Fig. 4; Cornamusini et al., 2017; Veneri, 1986). In the footwall of the Valmarecchia 'chaotic' units, rock types exposed to the west of the UMSTZ (refer to Fig. 1) include the carbonate to marly deposits accreted within the orogenic wedge. The outcropping stratigraphic succession starts with the Calcare Massiccio Fm. (carbonate platform limestone, Upper Triassic - Lower Jurassic) that represents the oldest formation exposed within the study area. This unit (unit 10 in Fig. 4) is overlain by the Jurassic-Lower Cretaceous series that is mainly composed of cherty limestone (Corniola Fm; unit 9 in Fig. 4) and pelagic micritic limestones (Maiolica Fm; unit 8 in Fig. 4). Calcareous-marly sediments deposited during the Late Cretaceous to Oligocene consist of marls (Marne a Fucoidi Fm; unit 7 in Fig. 4) and the Scaglia Group (unit 6 in Fig. 4). These sediments are covered by Miocene, hemipelagic deposits of the Bisciaro Fm. (Aquitanian -Burdigalian) and the Schlier Fm. (Langhian-Tortonian), both of which are mainly composed of alternating marly limestones, marls and shales (unit 5 in Fig. 4). Unit 4 includes turbiditic deposits that represent the fill of the Messinian foredeep, which developed to the east of the UMSTZ in response to the eastward migration of the thrust front (Ricci Lucchi, 1986). The deformed Messinian foredeep basin fill is presently preserved in the Marche foothills (Fig. 4). To the east, Plio-Quaternary strata composed of clays and sands (unit 3) and conglomerates (unit 2) cover the Messinian foredeep deposits, or locally rest unconformably directly on the calcareous-marly succession (Bigi et al., 1997; Cantalamessa et al., 1986; Cantalamessa and Di Celma, 2004; Ori et al., 1991). The contact between the Plio-Quaternary foreland basin succession and the older stratigraphic units is locally controlled by high angle faults (Deiana et al., 2002; Fig. 4).

4.3. Features of topography

In the UMAF, the low elevation and low-gradient foothills (to the east of the UMSTZ) pass to the mountainous landscape of the chain (to the west of the UMSTZ, Fig. 5). The location of the UMSTZ is marked, in the swath profiles of Fig. 6, by the sudden drop in the maximum, mean and the minimum elevation curves. This drop occurs at around 40 km in profiles 1, 2 and 3, and at around 30 km and 20 km in profiles 4 and 5, respectively. The foothills exhibit a smooth topography in the north (Fig. 5 and profiles 1–2 in Fig. 6) and a relatively rugged topography in the south (Fig. 5 and profiles 3 to 5 in Fig. 6). Valleys to the south are narrower and Pleistocene conglomerate deposits (unit 2 in Fig. 4), that are the stratigraphic cap of the foredeep section, are preserved in some remnants of paleosurfaces. Parallel to the foothills, the chain exhibits lower elevations and a smooth topography in the north. Here the highest peaks (e.g., Mt. Paganuccio, 976 m a.s.l.; Mt. Catria, 1702 m a.s.l.; Mt. Cucco, 1566 m a.s.l.; Mt. Murano, 882 m a.s.l.; Fig. 5 and profiles 1–2 in Fig. 6) correspond with the MR and the UMR formed by the Scaglia carbonate units (unit 6 in Fig. 4). The ridges are aligned along two distinct NNW-SSE trends that are separated by a large area where arenaceous and calcareous, marly, and clayey units crop out (units 4 and 5, respectively, in Fig. 4). Towards the south, the chain is more elevated and rugged. The MR and the UMR are separated by the Camerino Basin, where Messinian arenaceous deposits crop out, in the area spanning from the Esino R. to the Chienti R. valleys (Fig. 5 and profiles 2–3 in Fig. 6). The ridge to the NE (the MR) is carved in the Scaglia units (unit 6 in Fig. 4) and reaches a maximum elevation of 1021 m a.s.l. at Mt. Letegge (Fig. 5 and profile 3 in Fig. 6). To the SW, the UMR is carved both in the Scaglia and the Calcare Massiccio units (units 6 and 10, respectively, in Fig. 4) and its highest peak is Mt. Pennino (1571 m a.s.l., Fig. 5 and profile 3 in Fig. 6). Towards the south (from the Chienti R. to the Aso R. valleys) the MR and the UMR converge, and the chain exhibits its highest elevation with the peaks of Mt. Priora (2333 m a.s.l.) and Mt. Vettore (2467 m a.s.l., Fig. 5 and profiles 4–5 in Fig. 6), which are carved in the Scaglia and the Calcare Massiccio units (units 6 and 10, respectively, in Fig. 4). To the west of Mt. Vettore peak (profile 5 in Fig. 6),

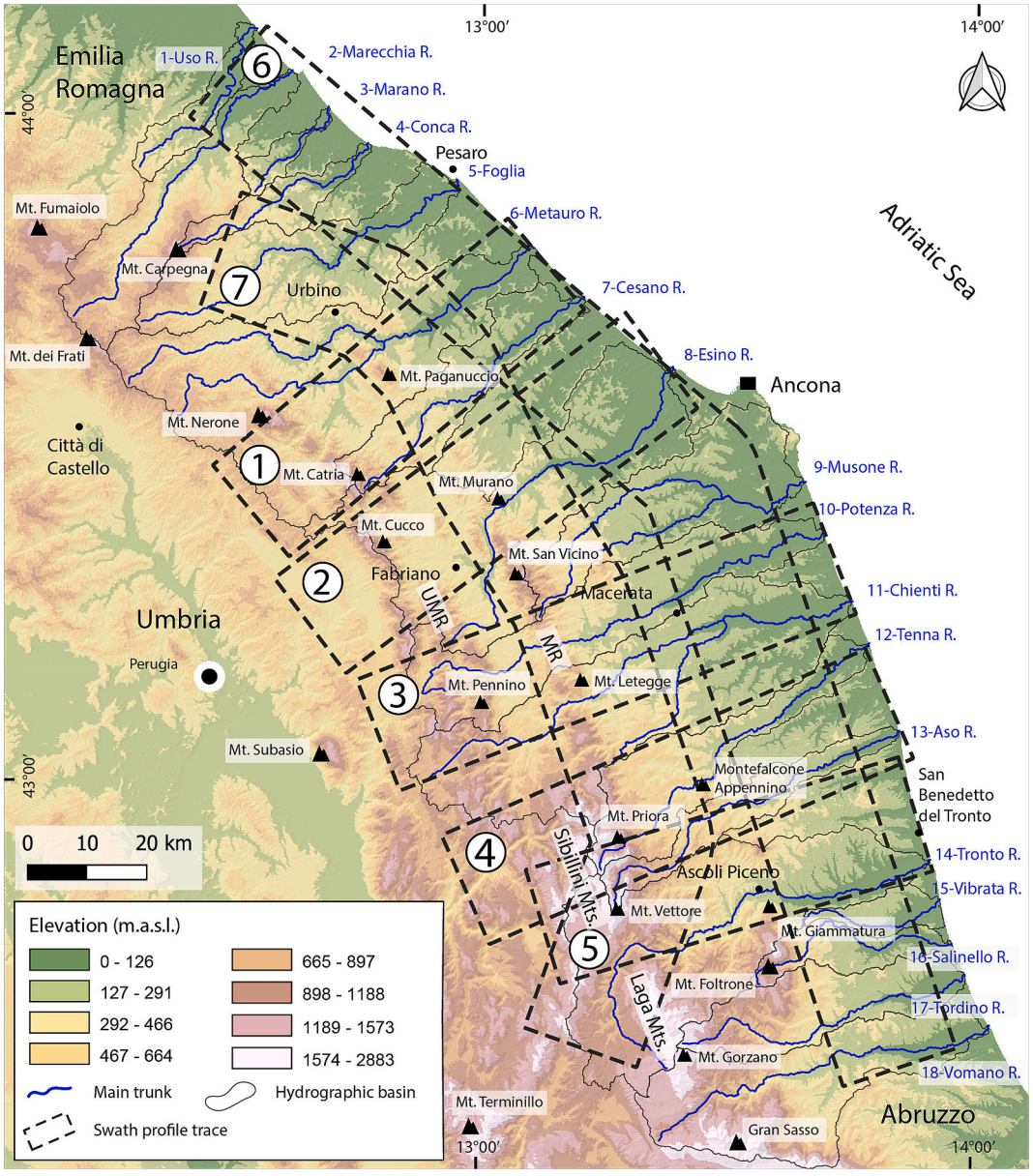

Fig. 5. Elevation map of the UMAF with location of the investigated main trunks, and correlative hydrographic basin. Black dotted boxes are the traces of swath profile in Fig. 6.

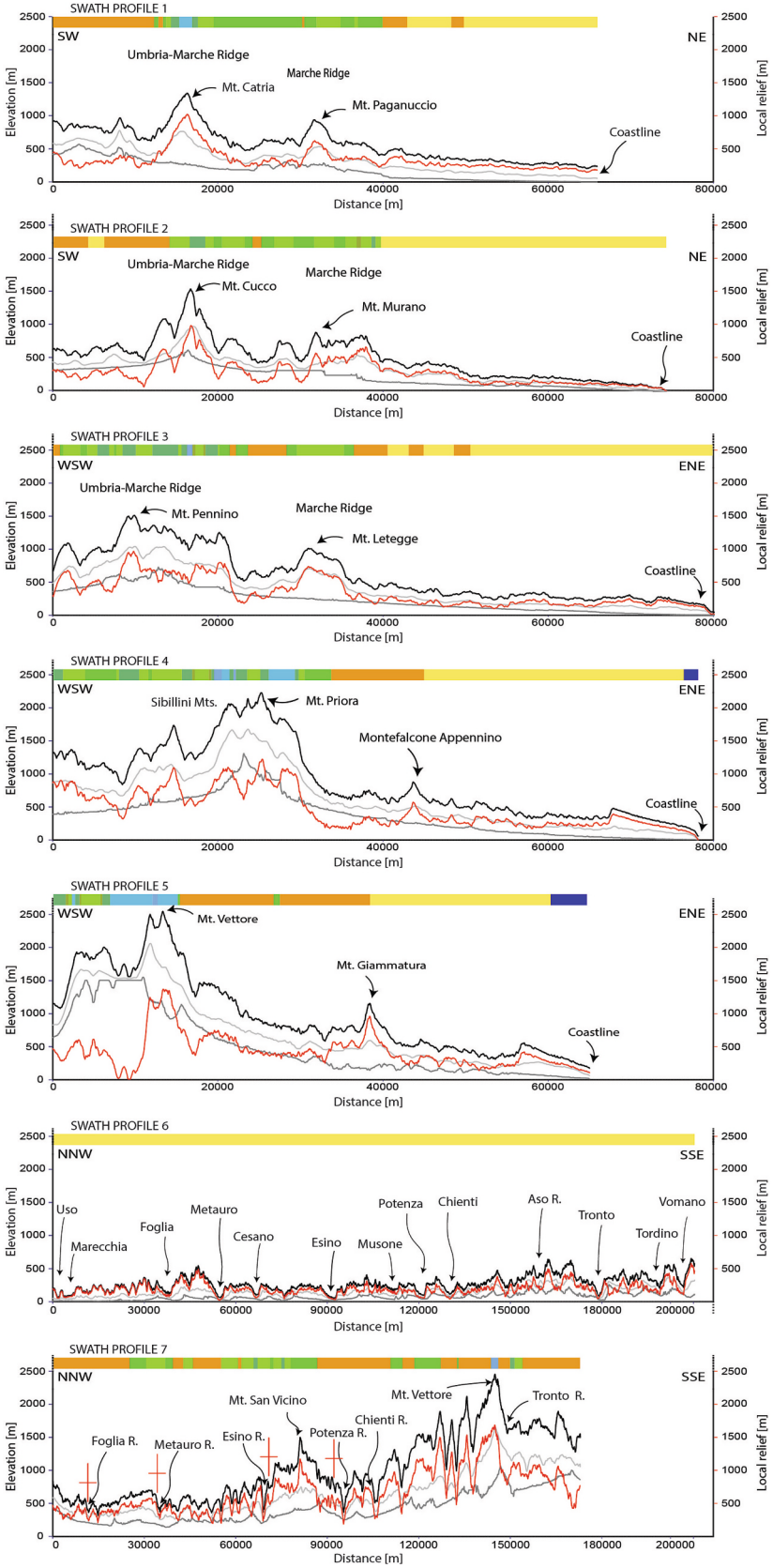

Fig. 6. Swath profiles within the Umbria-Marche Apennines and foothills (see Fig. 5 for the location). Swath profiles 1 to 5 are SW-NE trending and run perpendicular to the chain. Swath profiles 6 and 7 are parallel to the mountain front and perpendicular to river valleys. Black line indicates maximum elevation curve, gray line indicates mean elevation curve, light gray line indicates minimum elevation curve, and red line indicates relief curve. The colored bars above long river profiles represent the lithology of the bedrock reported in Fig. 4. Red crosses in swath profile 7 indicate location of the transverse faults mapped in Fig. 1. (For interpretation of the references to colour in this figure legend, the reader is referred to the web version of this article.)

high values in the maximum, mean and minimum elevation curves are coupled with low values in the relief curve. This feature is associated with the Castelluccio Quaternary basin in the hanging wall of the Mt. Vettore normal fault (Pierantoni et al., 2013). The southernmost portion of the investigated area (e.g., from the Tronto R. to the Vomano R. valleys), where Messinian arenaceous deposits crop out (unit 4 in Fig. 4), exhibits high to very high elevations that culminate in the peak of Mt. Gorzano (2458 m.a.s.l., Fig. 5).

Comparison of the profiles of Fig. 6 points to an overall increase of the elevation values towards the south (i.e., from swath 1 to swath 5). Such a trend is also evident by swaths 6 and 7 (Fig. 6), which run parallel to the foothills and to the outer sector of the orogenic belt, respectively. The highest peaks in the maximum elevation curves correspond with carbonate units, and this trend is mirrored by the mean elevation curves. The minimum elevation curve is smooth in the north (swaths 1, 2 and 3) with values not exceeding 500 m a.s.l., whereas in the south (swaths 4 and 5) it exhibits two relevant peaks exceeding 1000 m a.s.l. These peaks correspond with Mt. Priora (swath 4) and with the area to the west of Mt. Vettore (swath 5).

The relief curve mirrors the elevation curves, with the relief peaks that correspond with the highest elevation peaks, and with increasing local relief towards the south (i.e., from profile 1 to profile 5). Furthermore, swath profile 7 enhances the occurrence of three asymmetric, down to the north, broad paleovalleys that are now dissected by the more narrowly spaced transverse river valleys. The paleovalley to the north is centered around the Foglia River basin, the central one spans from the Metauro River basin to Mt. San Vicino, and the southernmost one extends from the Potenza River basin to Mt. Vettore.

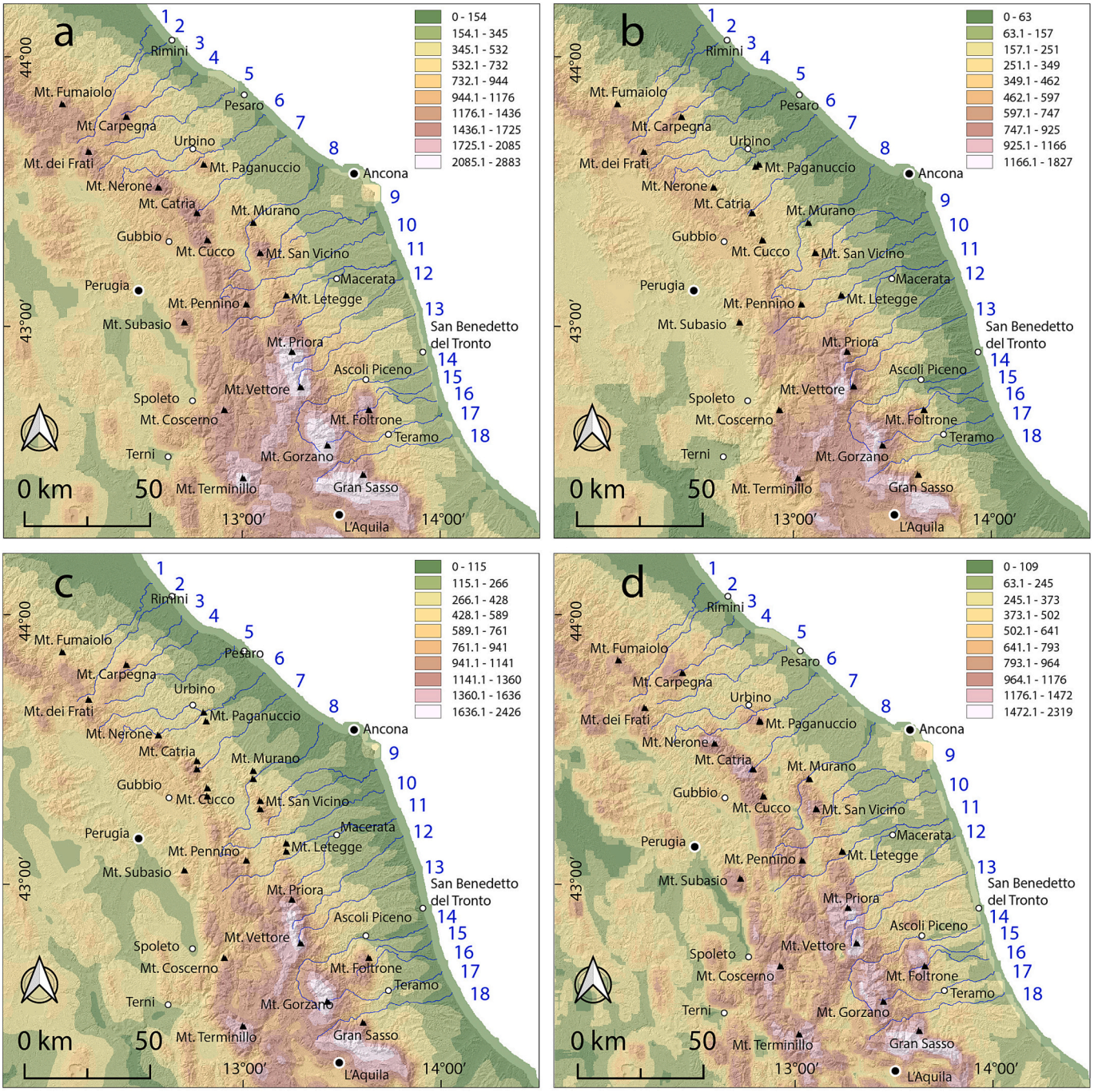

Fig. 7. Elevation maps of the study area. (a) Maximum elevation map. (b) Minimum elevation map. (c) Mean elevation map. (d) Local relief map.

The above-described topography setting is also highlighted by the maximum (Fig. 7a), minimum (Fig. 7b), and mean (Fig. 7c) elevation maps, as well as the local relief map (Fig. 7d). All these maps point to the presence of a locus of high elevations and high relief to the south of the investigated area (e.g., in the area between Mt. Vettore and Mt. Gorzano). This high elevation area spans from the west of the UMSTZ to the east of it and includes different rock-types, such as the carbonates of the Calcare Massiccio (unit 10 in Fig. 4) and the Messinian arenaceous deposits (unit 4 in Fig. 4).

4.4. River long profiles and chi-plot analysis

Figure 8 shows river long profiles and chi-plots of the eighteen investigated rivers. To construct the chi-plots, we adopted the best fit m/n ratio at the basin scale (Section 3.2). River long profiles and chi-plots exhibit variable features along the strike of the UMAF. In the northern sector, e.g., in the area between the Uso River and the Foglia River (rivers 1 to 5 in Fig. 8), chi-plots are rectilinear to slightly convex upward with the only exception of the Foglia River that exhibits a concave upward chi plot. Several knickpoints are identified. Using as a reference the lithological map of Fig. 4, some of the knickpoints have been classified as lithology-controlled knickpoints because of their proximity to contacts. These knickpoints occur along the Uso River, the Marecchia River and the Marano River (river 1, 2 and 3 in Fig. 8, respectively). On the opposite, knickpoints along the Conca River and the Foglia River (rivers 4 and 5 in Fig. 8) are not associated with lithological contacts (Figs. 8 and 9).

In the central sector of the investigated area, between the Metauro River and the Potenza River (rivers 6 to 10; Fig. 8), the chi plots are characterized by convex shapes with knickpoints that appear not associated with lithological contacts. However, a control by lithology may be hypothesized for the knickpoint that occurs along the Candigliano River (a right tributary of the Metauro River, 6; Fig. 8) to the west of Mt. Nerone (Fig. 9). Here the Calcare Massiccio (unit 10) outcrops in a deep gorge and passes laterally to marls, marly limestone and clay deposits of the Bisciaro, Schlier and Cinerea Fms. (unit 5).

Rivers in the southern sector of the study area (rivers 11 to 18 in Fig. 8) show chi-plots with shapes that vary from rectilinear and steep (11 - Fiastra River, a tributary of the Chienti River), to convex or slightly convex (15 - Vibrata River, 11 - Chienti River; 14 - Tronto River) and to rectilinear in the lower reach to convex upward in the upper reach (rivers 12, 13, 16, 17 and 18 in Fig. 8). Most of the widespread knickpoints identified along these rivers have been classified as non-lithology controlled knickpoints. Among the non-lithology controlled knickpoints, some in the upper reaches of the Chienti, Salinello, Tordino and Vomano Rivers (rivers 11, 16, 17 and 18 in Fig. 8), occur at short distances from normal faults. Knickpoints classified as lithology controlled are located along the Chienti (river 11, east of Mt. Letegge) and Aso (river 12, northeast of Mt. Vettore) rivers at contacts between units 6 and 4, and along the Tenna River (river 13, east of Mt. Priora) at the contact between units 5 and 6.

Figure 9 shows the spatial distribution of knickpoints. Most of the non-lithology controlled knickpoints are clustered in the southern sector of the UMAF (e.g., in the area spanning from the Tenna River to the Vomano River), and are mainly located to the east of the UMSTZ, where the Messinian arenaceous rocks (unit 4) crop out. Non-lithology controlled knickpoints located in the chain units to the south of the UMAF occur only along the Tenna River and the Aso River (number 12 and 13, respectively, in Figs. 8 and 9). On the opposite, to the north of the Chienti River valley, non-lithology controlled knickpoints are clustered to the west of the UMSTZ. Such knickpoints occur within the carbonate units, whereas knickpoints to the east of the UMSTZ affect just the Uso, Foglia and Musone rivers (number 1, 5 and 9, respectively, in Figs. 8 and 9).

Figure 10 shows chi-plots obtained with the average m/n value of 0.59. Chi-plots of rivers in the northern UMAF (sector A in Fig. 10) have mainly rectilinear shapes (rivers 1 to 6) with some slight convex upward segment in the upper reaches of rivers 2 and 4. In the central UMAF (sector B in Fig. 10, and rivers 7 to 10), chi-plots have rectilinear to slightly convex upward shapes. Rivers to the south of the UMAF (sector C in Fig. 10, and rivers 11 to 18) are characterized by overall steeper chi-plots, which show enhanced convex upward segments that locally pass to steep rectilinear segments in the lower reaches (rivers 11, 12, 13, 14, 16 and 17). By the diagrams it is evident that in sector C non-lithology controlled knickpoints occur at elevations $\geq$750 m and, however, higher than knickpoints in sectors A and B.

We have also derived a χ map of the study area, which is shown in Supplementary Fig. 1. Details on the spatial distribution of this index are reported in the caption of this figure.

4.5. Ksn index

Ksn values tend to increase towards the southwest, i.e., from the coastline to the foothills and to the mountain range (Fig. 11). Overall, the spatial distribution of the Ksn values follows the main features of the regional-scale topography. Low values are associated with the less elevated and low relief foothills, while the highest values are associated with areas characterized by high elevation and high local relief (Figs. 6 and 7). High Ksn values in the northern part of the study region are associated with the MR and the UMR. Between the ridges, areas with low Ksn values occur locally in correspondence of some tectonic depressions where arenaceous and Quaternary continental deposits outcrop.

Considering the dependence of the Ksn on bedrock erodibility (Section 3.2), and to better investigate the relationship between the outcropping rocks and drainage properties inferred from the long-profile analyses (Section 4.2), we constructed box plots of the Ksn values as a function of lithology, using as a reference the rock groups distinguished in Fig. 4 (Fig. 12).

By the compared box plots it appears that Ksn values respond to the lithological variability (Fig. 12). Although a net signature of each rock type is not identified, an association of the Ksn values with the lithological groups is evident. Overall, very low values are associated with the clastic deposits that outcrop in the foothills (units 2 and 3), with the lowest median value being associated with the clays and sands. Higher values characterize the mountain range units. For instance, in the entire study region, the highest Ksn values are associated with the carbonate rocks of the Maiolica and Corniola Fms. (units 8 and 9) and particularly, with the massive limestones of the Calcare Massiccio Fm. (unit 10). The marly and clayey rock-types (namely, units 5, 6 and 7) that are part of the Mesozoic-Cenozoic succession are coupled with lower Ksn values. The Messinian arenaceous deposits (unit 4) exhibit low Ksn values that are comparable with those of the marls, marly limestone, and clays of the Schlier, Bisciaro and Cinerea. Fms. (unit 5).

The map of Fig. 11 also shows that the Ksn values are affected by an along-strike variability and, particularly, increase from sector A to sector C. To analyze the pattern of the along-strike Ksn variability, we applied the box plot analysis as a function of lithology to each of the three sectors identified by the chi plot analysis (Fig. 13). The comparison of box plots constructed for sectors A, B and C indicates that, substantially, the statistical distribution of Ksn as a function of the lithological groups outcropping in the entire study area (and, particularly, the trend of the median values) is maintained in each of the sectors. In addition, the comparison between sectors A, B and C indicates that, for each rock type, the median value increases from sector A to sector C.

4.6. Spatial variation of the erodibility parameter (K)

Values of the erodibility parameter (K) are reported in Table 1 and Fig. 14. This index has been calculated only for the drainage basins for which erosion rate estimation are reported in literature. The analysis points to a similar average Ksn value from the Marecchia River to the Chienti River (i.e., Ksn between 30 and 40), with the only exception of

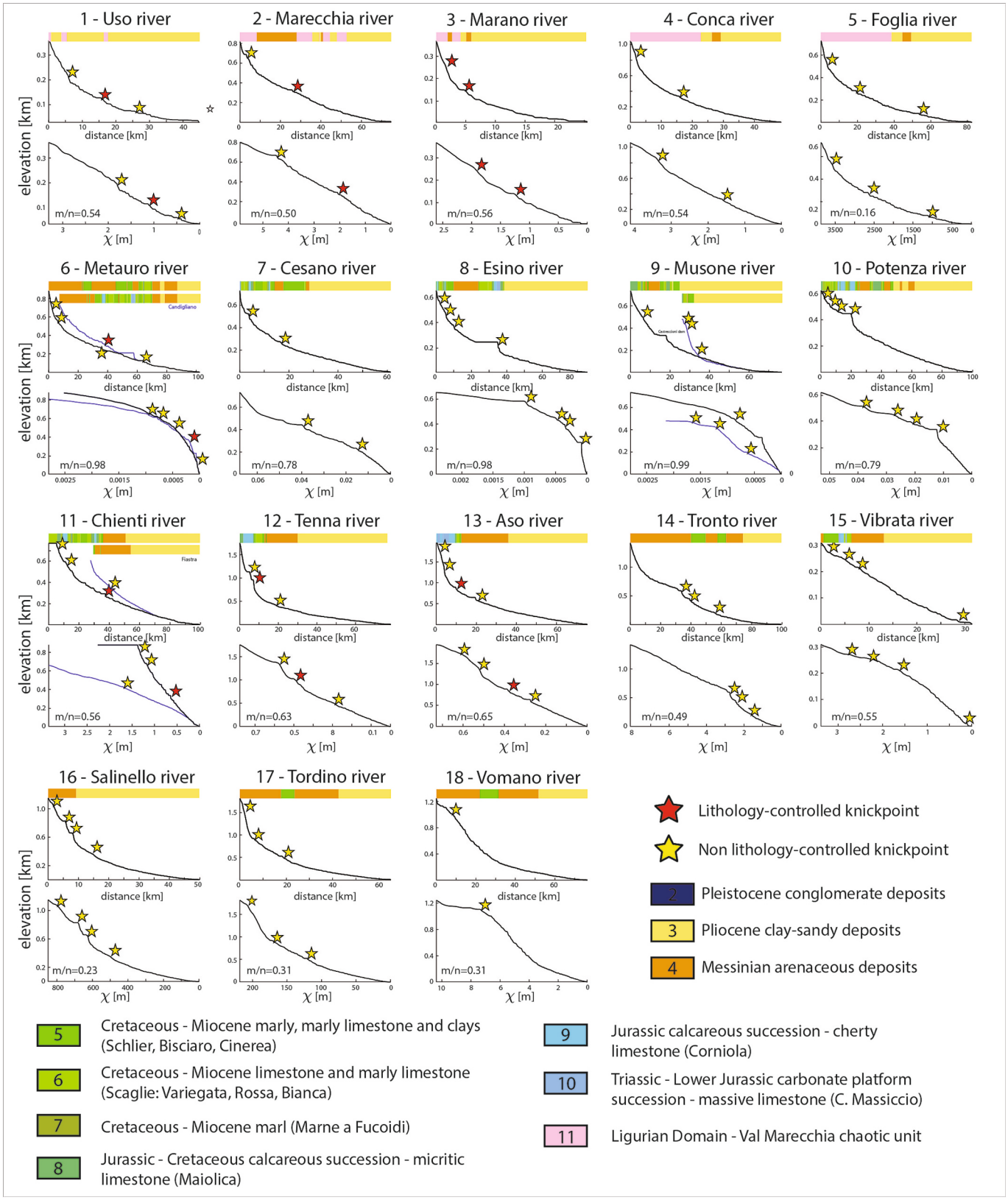

Fig. 8. Longitudinal profiles and chi plot of the 18 rivers analyzed in the present work. Chi-plots have been constructed using the best fit m/n ratio at the basin scale. The colored bars above long river profiles represent the lithology of the bedrock reported in Fig. 4.

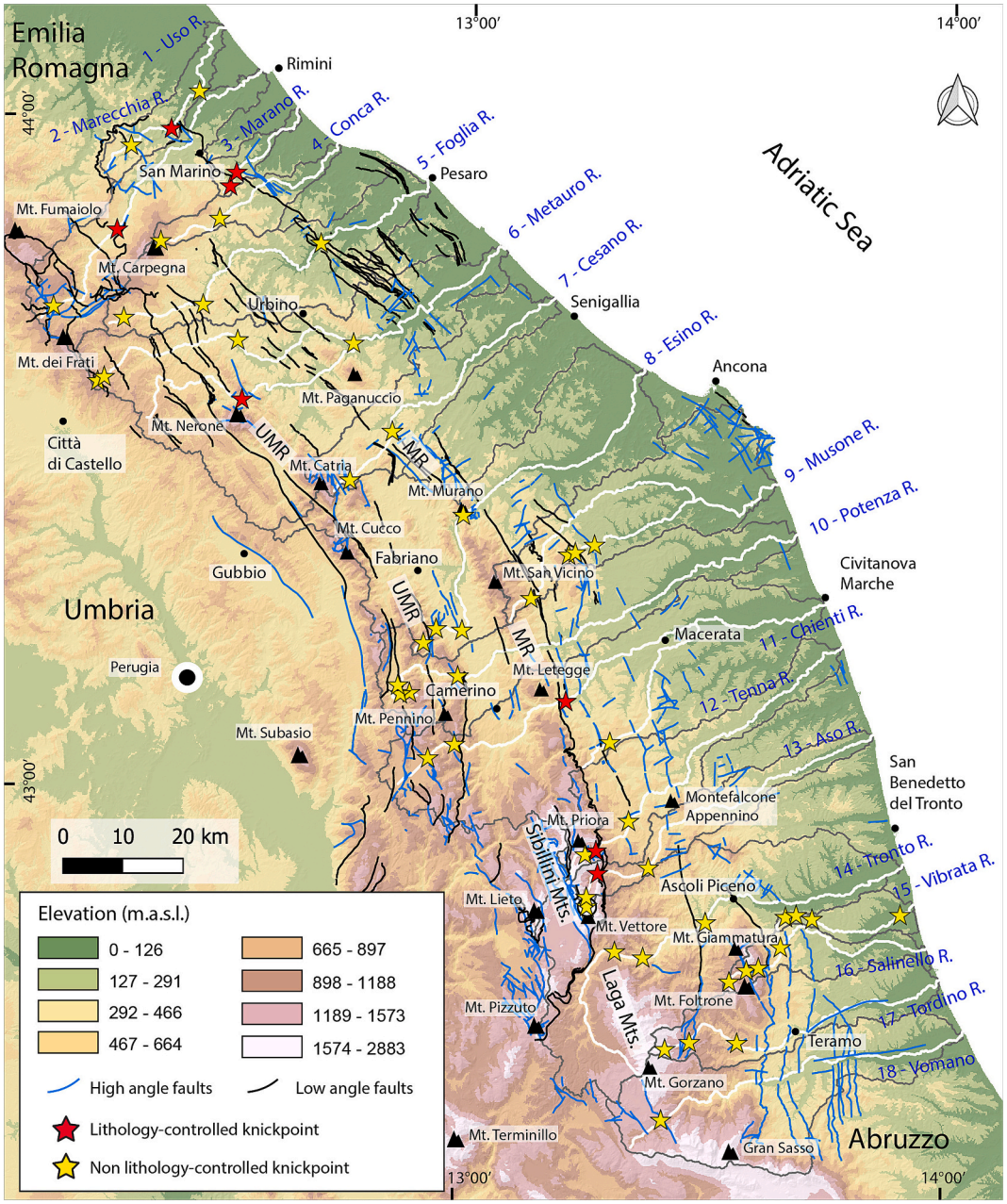

Fig. 9. Topographic map showing the knickpoints/knickzones spatial distribution along the 18 river channels analyzed in the study area. The identified knickpoints are distinguished in lithology-controlled knickpoints and non-lithology-controlled ones, using as a reference the geological map of Fig. 4. In this regard, red stars represent sharp change in channel slope due to lithological contrast while yellow ones are the knickpoints related to possible base level perturbation. (For interpretation of the references to colour in this figure legend, the reader is referred to the web version of this article.)

the Musone River that exhibits the lowermost value (Ksn value of 10.8). The Tronto River is characterized by the highest average Ksn value, this being almost double the value of rivers to the north of it. Erosion rate values range between 0.2 mm/yr (Musone R.) and 0.38 mm/yr, with the highest values in the Tronto River basin (0.6 m/yr^{-3}). The erodibility (K) parameter exhibits similar values among all the analyzed drainage basins except for the Musone River, where it doubles the other values.

5. Discussion

In our study, we performed an analysis of topography and river network of the Adriatic slope of the Umbria-Marche Apennines using multiple metrics and indices. We calculated the spatial distribution of elevation and parameters of the drainage network, i.e., river steepness and χ index, and compared these metrics with the outcropping rock types. Such an approach provided us with a key to unravel the tectonic vs. lithological signals and to identify areas with different behaviors in terms of vertical motions.

5.1. Lithological control on topography and drainage network features

The spatial coincidence of high vs. low values of parameters such as elevation and local relief with outcrops of carbonate rocks (e.g., along the MR and the UMR) and clayey and/or arenaceous rocks (e.g., the Camerino basin; Figs. 6 and 7), respectively, is a feature that the UMAF share with other sectors of the Apennines. Like the central and southern Apennines (Ascione and Cinque, 1999; Ascione et al., 2008; Buscher et al., 2017; Lanari et al., 2023; Pazzaglia and Fisher, 2022), it appears

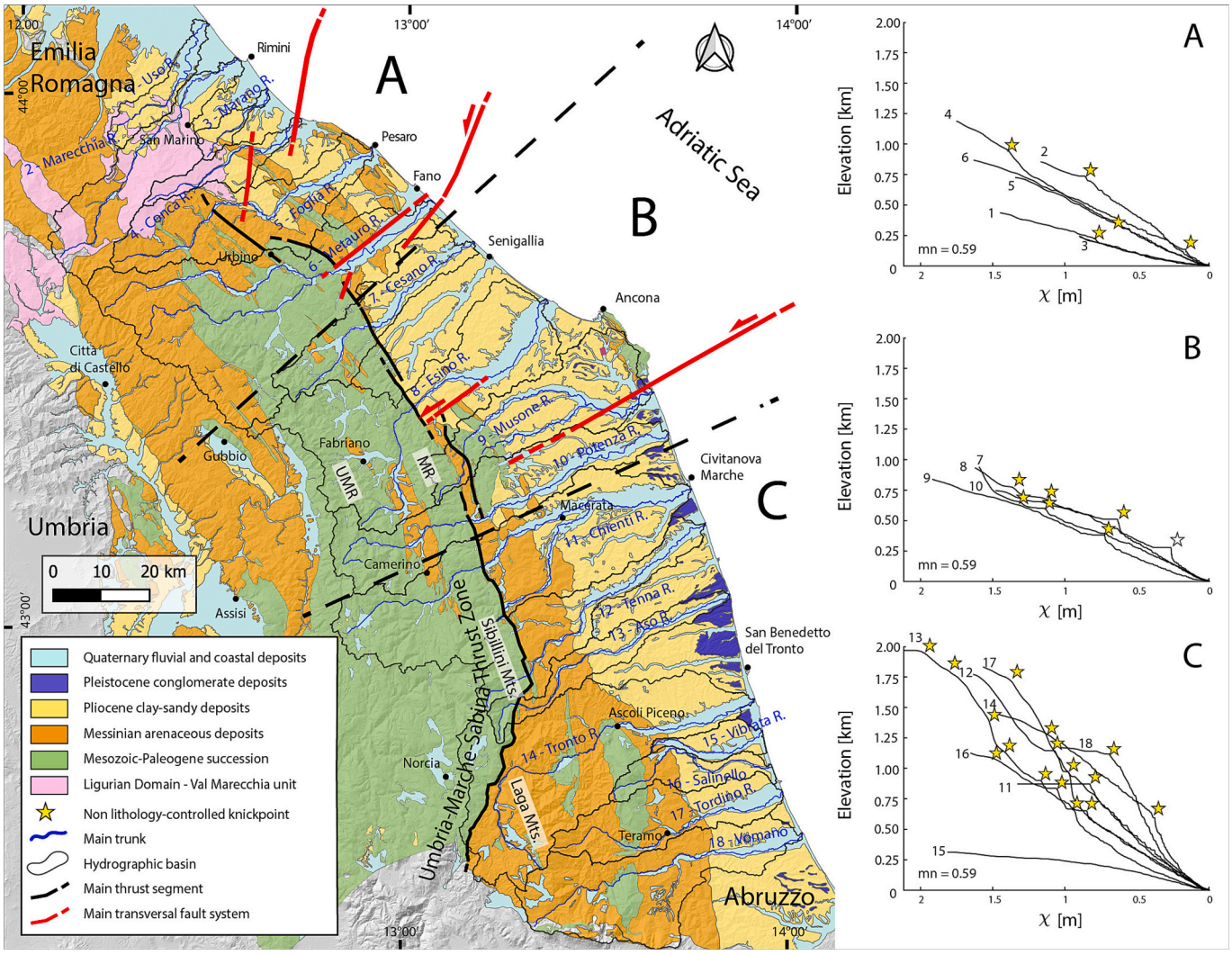

Fig. 10. Geological sketch of Umbria-Marche Apennines and foothills (modified from Conti et al., 2020) with the major transversal structures (modified from Costa et al., 2023 and Pierantoni et al., 2019). On the right, chi plots of the main rivers of hydrographic basins (locations and numbering in Fig. 5), constructed using a best fit m/n value of 0.59. Non-lithology-controlled knickpoints are also reported.

that bedrock lithology exerts a strong control on the features of topography of the UMAF mountain range.

The same is also inferred from the analysis of river long-profiles, which are well known to respond to the control exerted by lithology (e.g., Duvall et al., 2004; Pazzaglia et al., 1998; Stock and Montgomery, 1999). The extent to which the nature of the bedrock affects the features of the drainage is inferred from the statistical analysis of the Ksn values (Fig. 12). This analysis, consistently with findings from various morphoclimatic and morphotectonic settings (Bernard et al., 2019; Clementucci et al., 2022; Seagren and Schoenbohm, 2019), indicates that such a parameter is influenced by the resistance to erosion of the bedrock. In our instance, the Ksn box-plot analysis allows a net distinction between the carbonate rocks of the Maiolica, Corniola and Calcare Massiccio Fms. (units 8, 9 and 10; Fig. 12), which are all characterized by high Ksn values, and rocks composed of arenaceous and marly-clayey lithologies (unit 4; Fig. 12). Therefore, it is evident that the carbonate rocks of the Mesozoic-Paleogene Umbria-Marche succession (namely, the Maiolica, Corniola and Calcare Massiccio Fms.) respond to erosion as hard rocks relative to the softer marly-clayey portion of the same succession (namely, the Schlier, Scaglia, and Bisciaro Fms.) and the Messinian sandstones. The only exception is the very low Ksn values associated with the Calcare Massiccio (unit 10) in sector A. These low values are due to the limited areal distribution of the Calcare Massiccio that outcrops at low elevation just in some gorges carved by the Metauro river (river 6). This implies that the low Ksn values associated with the Calcare Massiccio in sector A are mainly affected by elevation and local relief rather than lithology.

The coupled variations of the Ksn, elevation and relief parameters with lithology are indicative of the main role exerted by differential erosion in the formation of the landscape of the uplifting UMAF, as it has been inferred for the northern Apennines (Erlanger et al., 2021) and Crete (Ott et al., 2019). However, the variability of bedrock lithology in the UMAF is much greater across than along the strike of the investigated region (Fig. 4). This suggests that the along-strike variation in topography and river network features may be considered as less affected by outcropping rock types.

Consistently, the erodibility parameter (K) exhibits similar values from north to south despite the southward increase in the erosion rate and in the average Ksn at the basin scale (Table 1 and Fig. 14). Therefore, the jump in Ksn values towards the south appears not merely correlated with variable bedrock types. The only exception is the Musone River basin that exhibits low Ksn value, erosion rate like the other investigated basins and the highest erodibility (Fig. 14). This feature relates to the occurrence of a bedrock mainly composed of foredeep units (Fig. 4) in contrast with the other investigated basins, which are mainly carved in the chain units.

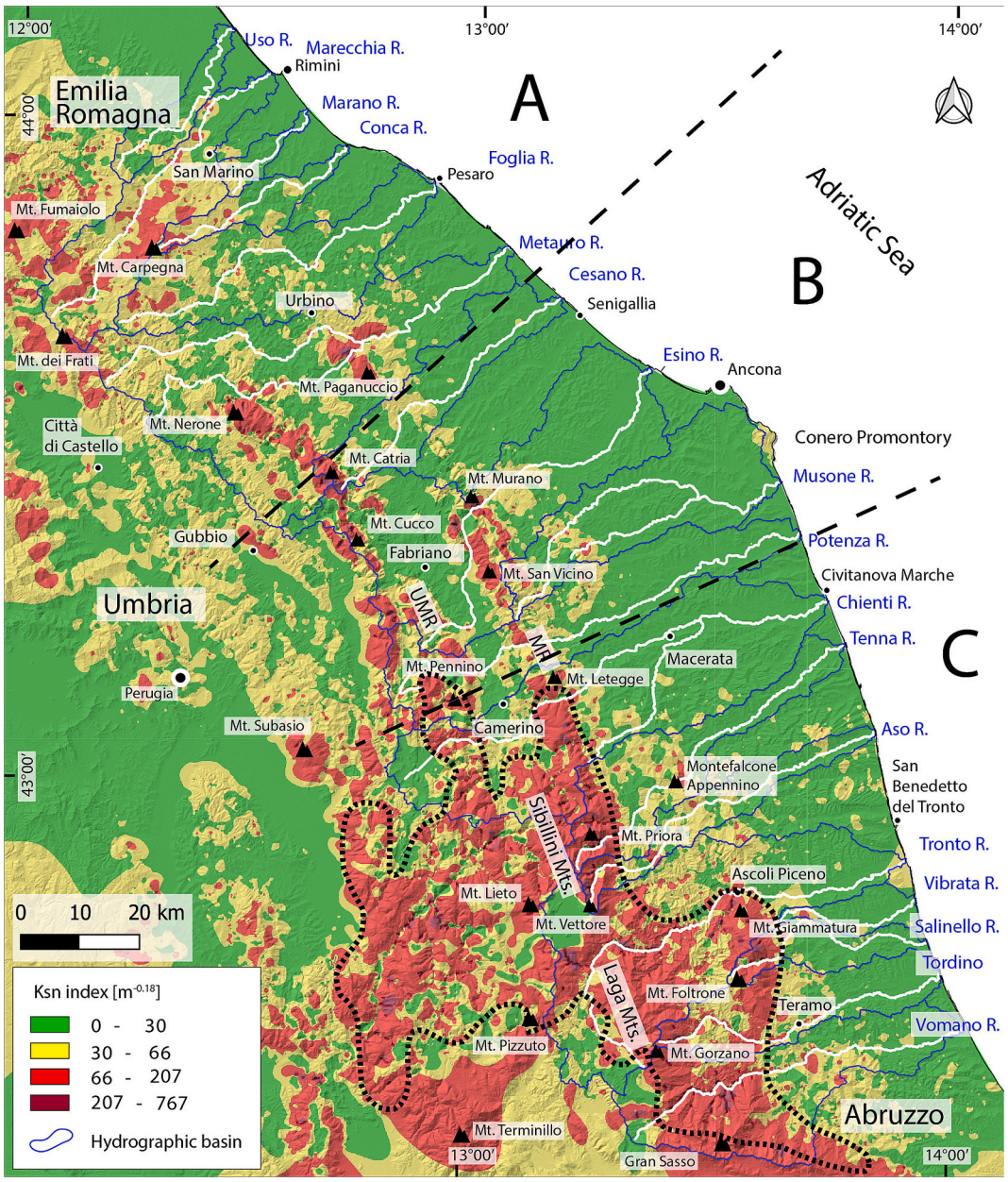

Fig. 11. Spatial distribution of Ksn index. Dashed black line limits the high Ksn value area. The sectors A, B and C of Fig. 10 are also reported.

5.2. *Along strike variation of uplift*

Elevation and its derivative parameters described in Section 4.3 all increase towards the south, with maximum values occurring in the Sibilini Mts. and the Laga Mts (Figs. 5, 6 and 7). This area corresponds with the high Ksn area shown in Fig. 11. The locus of high elevation, high relief and high Ksn values to the south of the UMAF includes both carbonate rocks (units 8, 9 and 10 in Fig. 4), which culminate with the peak of Mt. Vettore, and arenaceous rocks that peak with Mt. Gorzano (unit 4 in Fig. 4). The southward increase in Ksn values is clearly imaged by the box plots in Fig. 13, which show a jump of this metric for all rock types in the southern portion of the UMAF. Noteworthy, Ksn values associated with the Messinian arenaceous units (unit 4) in sector C, besides being much higher than the correlative values in sectors A and B, approach the Ksn values of calcareous and marly units (units 5, 6, 7 and 8).

This, in turn, supports the idea that lithology is not the first controlling factor in the southward increasing elevation and in the steepness of the rivers (and chi plot patterns), consistent with analyses by Lanari et al. (2023)that demonstrated that lithology alone cannot explain the remarkable differences reported along the Apennines (e.g., elevation, river steepness, etc.). Therefore, by our datasets it can be inferred that the southern portion of the study area experienced larger uplift. This agrees with the findings of Racano et al. (2024) that recognized a southward increasing trend in rock uplift in the central Apennines, with a maximum in the area around the Sibillini Mts.

Focusing on the tectonic evolution of the UMAF (Section 2), the larger uplift recorded in the southern part of the study area bears components related to both syn-orogenic shortening and post-orogenic extension (e.g., the high elevation of Mt. Vettore peak). These two components are not easily isolated, although the distribution of horizontal displacement associated with the UMSTZ, which shows a marked maximum in the southern Marche region (~ 10 km in the Mt. Vettore area) and values not exceeding 5 km in the northern Marche region (Mazzoli et al., 2005), suggests that thrusting played a major role in producing structural elevation. Therefore, the larger uplift experienced

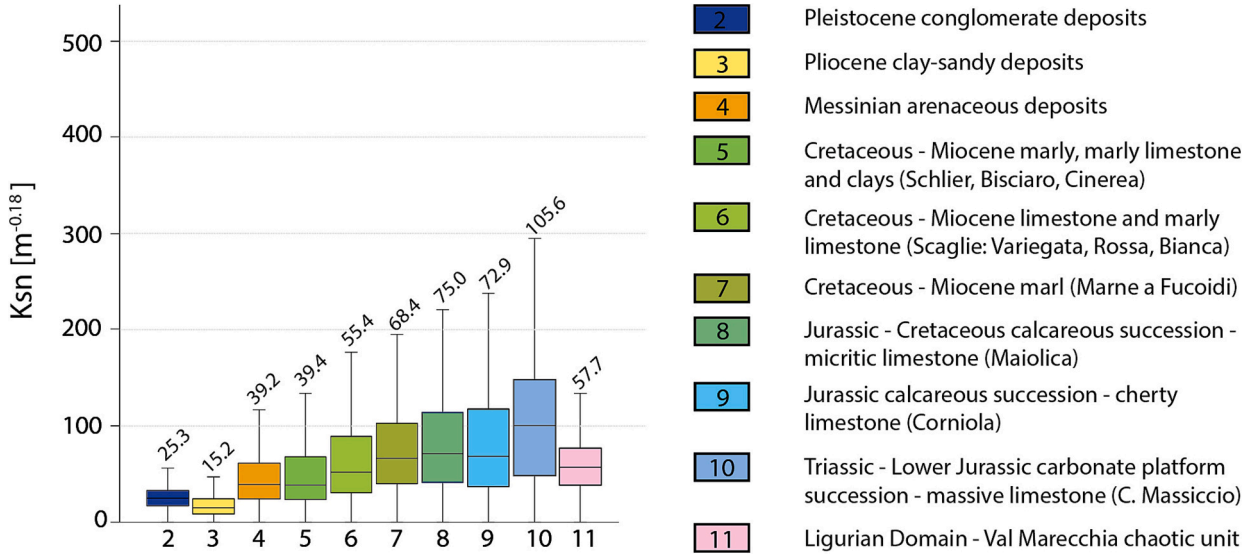

Fig. 12. Box plots showing distribution of the Ksn value as a function of lithology. The mean of the distribution is shown by the horizontal line within the box and it is repeated as the number above the top whisker. The top and bottom of the box are the 75th and 25th percentiles and the whiskers are the 95th and 5th percentiles.

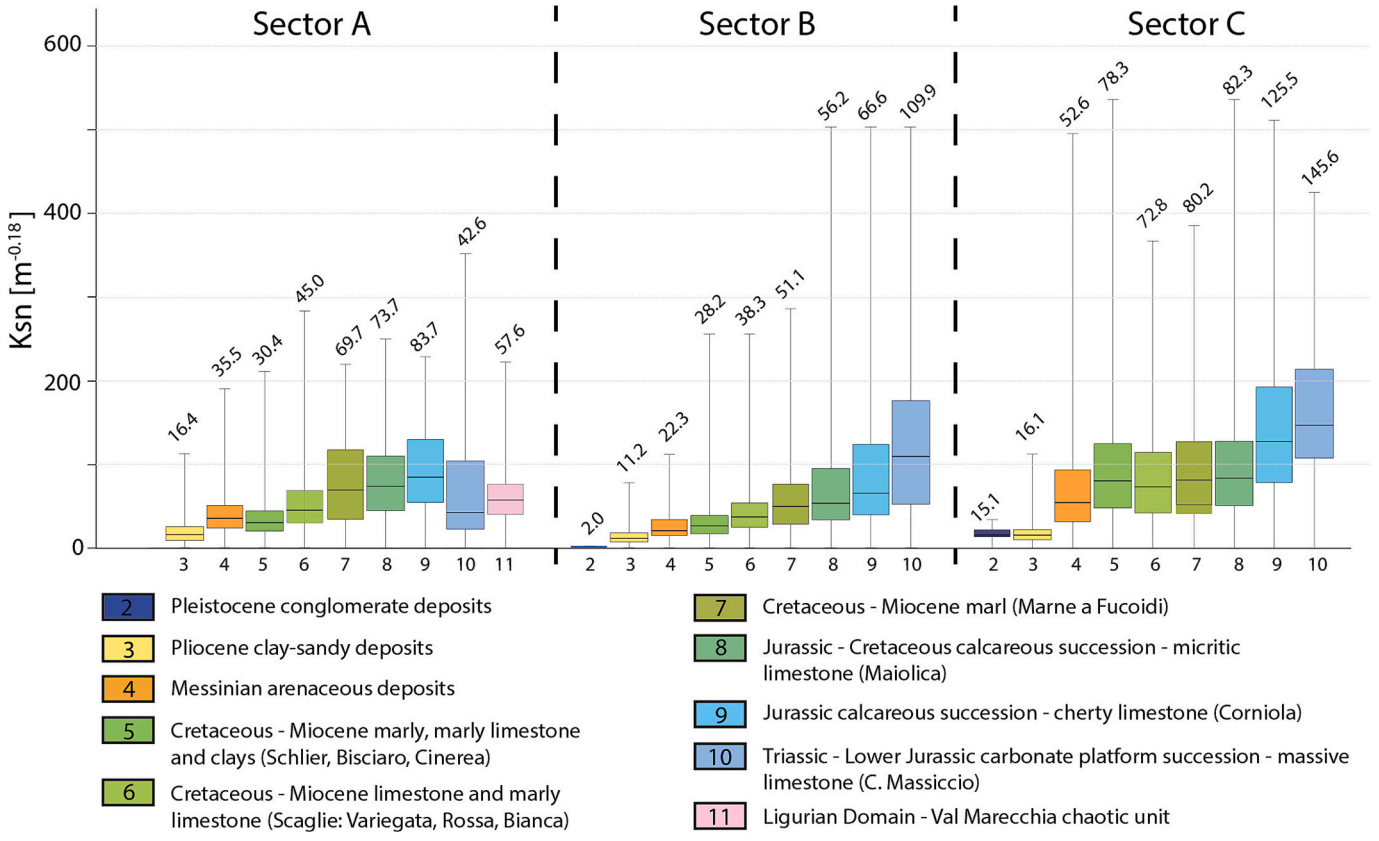

Fig. 13. Box plots showing Ksn value as a function of lithology. Numbers on top of each box plot indicate the median value.

by the southern UMAF is partly inherited from pre-Quaternary times, as it is also observed in the central Apennines more to the south (Ascione et al., 2008). However, parameters of the drainage net, which is particularly sensitive to recent/active tectonic perturbations (Kirby and Whipple, 2001; Racano et al., 2021; Whittaker et al., 2008), all support the idea that the southward increase in surface uplift has continued during the Quaternary times. Collectively, parameters such as non-lithology controlled knickpoints and Ksn index and their spatial distribution, and chi-plots (Figs. 9, 10, 11 and 13), all indicate that rivers in the southern portion of the UMAF are more perturbed relative to other rivers. Within such a regional-scale trend, the stepped positions – independent from bedrock lithology - of the bottoms of the three broad paleovalleys identified in swath profile 7 (Fig. 6; Section 4.3) suggest a discrete more than gradual elevation increase towards the south. Discrete jumps in elevation occur at the boundaries between sectors (A, B, C; Fig. 10) of the UMAF that feature different drainage net metrics.

Table 1
Values of the erodibility parameter (K) for some of the investigated drainage basins.

Drainage basin	Average Ksn ($m^{0.18}$)	Erosion rate (mm/yr)	Error	K ($m^{1.18}$/yr x 10^{-3})	Error	Source
Marecchia River	31.25	0.21	± 0.03	0.00672	± 0.00096	Guerra and Lazzari (2020)
Metauro River	39.65	0.38	± 0.03	0.009584	± 0.000757	Nesci et al. (2012)
Esino River	34.13	0.25	± 0.05	0.007325	± 0.001465	Nesci et al. (2012)
Musone River	10.8	0.2	± 0.002	0.018519	± 0.000185	Wegmann and Pazzaglia (2009)
Chienti River	38.44	0.35	± 0.03	0.009105	± 0.00078	Wegmann and Pazzaglia (2009); Coltorti et al. (1991)
Tronto River	60.69	0.6	± 0.02	0.009886	± 0.00033	Sembroni et al. (2020)

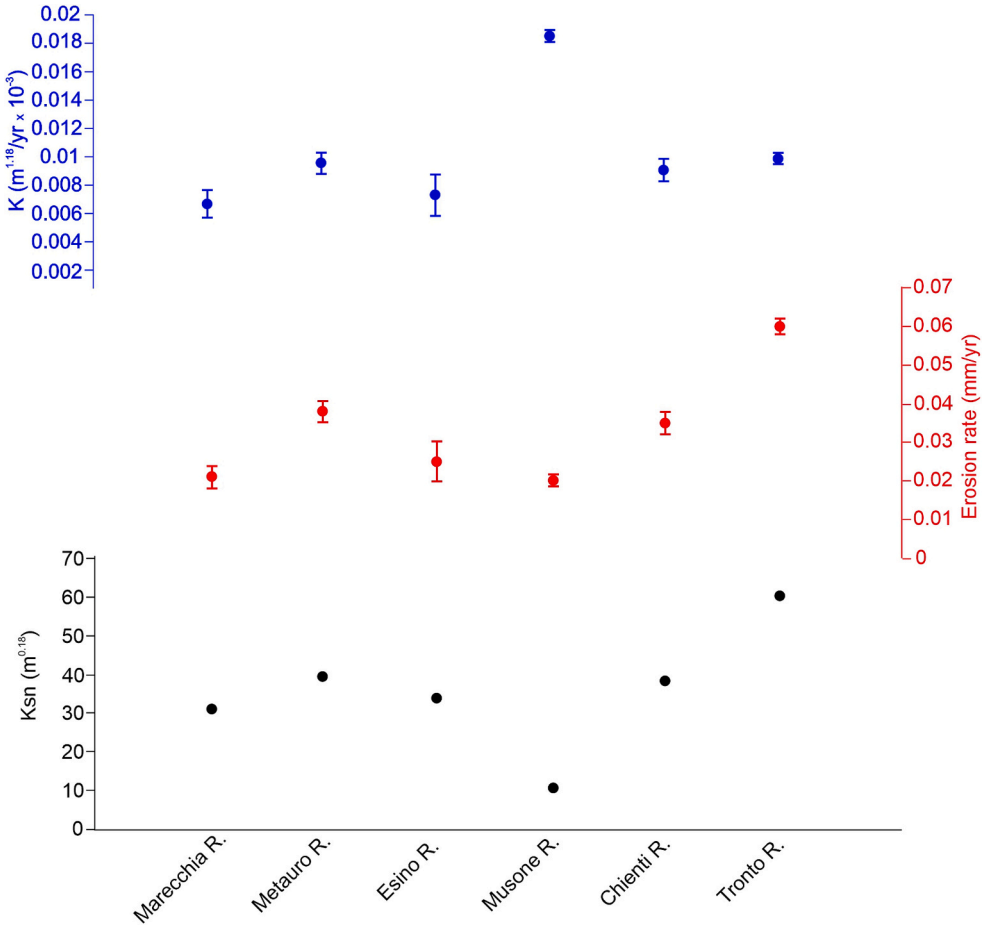

Fig. 14. Distribution of the Ksn, erosion rate and erodibility (K) among the selected drainage basins. Drainage basins are listed from north to south.

Sector A is characterized by the lowest values of Ksn index (Fig. 13) and by rivers (rivers 1 to 6; Figs. 8 and 10) that feature smooth long-profiles and rectilinear chi plots (Fig. 10), which suggest that those rivers are substantially keeping pace with subdued uplift. In sector B the Ksn index is characterized by mean values and river chi-plots (rivers 7 to 10; Figs. 8 and 10) that register only some minor perturbation and are not far from keeping pace with moderate uplift. Sector C includes the high Ksn area (Figs. 11 and 13) and river chi-plots that are either overall convex upward or with convex upper reaches that pass to steep rectilinear lower reaches (Fig. 10). Considering the large sizes of the convex upward reaches, the variable nature (carbonate and arenaceous) of the bedrock that is incised, and the abundance of non-lithology controlled knickpoints, the nature of the transient signals in the rivers that dissect sector C is reasonably correlated with tectonic signals. These are not merely correlated with extensional faulting, as the across-strike size of the area subject to faster uplift encompasses the area affected by normal faulting and extends eastwards to involve the deformed foredeep. The transformed profiles of rivers in Sector C, relative to those located more to the north in the UMAF, are generally steeper even in their straight lower reaches. Such a feature would suggest (e.g., Perron and Royden, 2013) a tendency of rivers 11 to 18 to the attainment of equilibrium with uplift faster than those one affecting the area to the north of sector C., This is consistent with estimates for the Chienti and Tronto rivers basins by Sembroni et al. (2020) and Pazzaglia and Fischer (2022). Accordingly, transient signals in Fig. 10 are clustered at higher elevation ($\geq$ 750 m) in sector C compared to sectors A and B. Assuming that knickpoints record the same unsteady base level fall history, the difference of elevation of transient signals in sectors A and B compared to sector C is indicative of uplift of sector C greater than uplift of sectors A and B.

Overall, our results are consistent with findings of recent works (e.g., Faccenna et al., 2014; Fellin et al., 2022; Lanari et al., 2023; Serpelloni et al., 2013; Racano et al., 2024) pointing to a southward increase of uplift. These papers interpret the uneven uplift in terms of deep geodynamic processes, without discussing the role of crustal transverse structures. Dynamic support may not have a unique topographic fingerprint and if anything, the more parsimonious explanation is that

crustal structure changes significantly across NE-SW oriented zones, and it is this crustal structure and crustal processes that are a better explanation for the observed geomorphology. Our data provide new insights in the uplift pattern, being indicative of a compartmentalization of the UMAF that is consistent with the occurrence of transversal lineaments controlling differential uplift. Crucial to unravel such a behavior of the UMAF were the (i) analysis of the along-strike features of elevation (i.e., swath n. 7 of Fig. 6), (ii) mutual comparison among river network metrics, in particular chi-plot shapes and elevations of transient signals (Fig. 10), (iii) box plots and whisker plots of Ksn values as a function of lithology (Fig. 13), and (iv) recognition of the net jumps of those metrics at the well-identified positions.

5.3. The role of transversal structures

Transversal structures are well known to occur in orogenic systems all over the world, including the Apennines (Pascucci et al., 2007). The scale of these structures varies from the common tear faults associated with individual thrust sheets and confined within thrust hanging-wall blocks (Dahlstrom, 1970), to plate-scale transform faults. Within this wide range of scales, fold and thrust belts may be compartmentalized by crustal or even lithospheric structures that are not manifested by discrete fault zones at the surface but are unraveled by geophysical data and/or geomorphological evidence. Tearing of the subducting slab and related focusing of the slab pull force could result in transversal lithospheric structures impacting fold and thrust belt geology and geomorphology (e.g., Handy et al., 2019, and references therein). This may be the case of the northern-central Apennines, where a southward increasing uplift rate has been attributed to local slab detachment beneath the central Apennines since late Pliocene/early Pleistocene times (Faccenna et al., 2014; Fellin et al., 2022). Marked along-strike variations of relief evolution could also result from delamination of the Adria lithosphere, a process recently inferred by Menichelli et al. (2023) based on seismic tomography. In this model, belt topography is dynamically sustained by mantle substitution generated during the delamination process. According to the latter authors, delamination proceeded with different retreat velocity along the mountain belt. The resulting irregular geometry could have triggered belt segmentation, producing different sectors bounded by transversal structures.

The geodynamic processes discussed above may well play a role in along-strike segmentation of the northern-central Apennines. However, greater uplift in the southern sector of the UMAF, evidenced by recent literature and the analysis completed here, appears to be essentially controlled by inherited (Late Miocene to Pliocene) crustal scale shortening rather than dynamic support. The basement-involved thrust architecture of the mountain belt (Fig. 2) is fully consistent with such an interpretation. Within our study area, the boundaries among sectors (A, B, C) characterized by different active tectonic behavior, roughly coincide with major transversal faults segmenting the outer portion of the fold and thrust belt in the Marche foothills and adjacent offshore area (Fig. 1). This correlation suggests that such transversal 'lineaments' mark the loci of long-lived, deep-seated fault zones that exert a major control on the active tectonic behavior of large crustal blocks. The recent reactivation of inherited, transversal crustal faults in the foreland plate has been unraveled in the southern Apennines by Bitonte et al. (2021). The latter authors also documented fault propagation into the foreland basin deposits as a result of basement fault reactivation. A similar process is envisaged to have occurred also in the present study area, where pre-existing, deep-seated transversal faults of the foreland plate appear to have controlled fold and thrust belt propagation and related segmentation of the deformed Plio-Pleistocene foredeep (Centamore and Nisio, 2003; Costa et al., 2021; Costa et al., 2023; Pierantoni et al., 2019). Long-term activity of such transversal faults likely involved: (i) their development during Triassic to Early Jurassic times as extensional/oblique-slip faults within the framework of continental rifting (e.g., Tavarnelli et al., 2019); (ii) their reactivation as strike-slip/oblique-slip faults compartmentalizing the fold and thrust belt during forelandward migration of shortening (Calamita et al., 1994; Calamita and Pizzi, 1994); and (iii) their reactivation as extensional/oblique-slip faults in the hinterland of the eastward migrating fold and thrust belt. Stages (ii) and (iii) above are both Neogene-Quaternary in age, extension following shortening in both space and time. The results of this study document the influence of the transversal lineaments on the drainage network and topography of the study area.

The fact that the crustal sectors (A, B, C) characterized by different active tectonic behavior extend SW-ward into the axial zone of the mountain chain (i.e., also in the hanging wall of the major thrust – the UMSTZ – that defines the mountain front), further suggests that the transversal 'lineaments' mapped in the frontal part of the fold and thrust belt mark major crustal structures extending beneath the high mountain chain. As the latter area is presently dominated by ongoing extension, it may be envisaged that the deep-seated transversal structures interact with the active normal faults, thus segmenting the Quaternary extensional system in the axial zone of the chain. This is consistent with seismicity distribution, and with the abrupt northward truncation of the events associated with the 2016–2017 Amatrice-Visso-Norcia and the 1997 Colfiorito seismic sequences (Fig. 3) along the boundary between block C and block B in Fig. 10. Moreover, recent studies based on instrumental seismicity (Mazzoli et al., 2014, 2015), seismic interpretation (Costa et al., 2021) and paleoseismological evidence (Materazzi et al., 2022) highlight that major transversal structures can also host moderate to significant seismic events (e.g., the Mw 6.17, 1741 Fabriano earthquake; the Mw 4.68, 1972 Ancona earthquake). The transversal structures are a likely source of these large Marche earthquakes that have no obvious correlation to emergent normal or thrust faults.

6. Conclusions

A morphotectonic analysis of the topography and drainage network features was applied in this study to discern the lithological and tectonic signatures on landscape evolution in the Umbria-Marche Apennines and Foothills (central Italy). Topography and river network features exhibit along-strike variations that are consistent with a southward increase of surface uplift rather than bedrock variability. Differential uplift associated with three major crustal blocks was identified, with surface uplift reaching its maximum in the southernmost one (Sibillini Mts. – Laga Mts. area). Crucial to the detection of the UMAF uplift pattern was the identification of discrete variations in the metrics we analyzed.

In the Marche foothills and Adriatic offshore, the boundaries among crustal blocks characterized by different active tectonic behavior roughly coincide with major transversal faults recently mapped by seismic interpretation. Our study indicates that the crustal blocks displaying differential surface uplift extend westward into the axial zone of the mountain chain, which is characterized by active extension and associated intense seismicity. Seismicity distribution, including the pattern of the 2016–2017 earthquake sequence, is consistent with a compartmentalization of the active extensional fault system in the axial zone of the mountain chain. Therefore, it may be envisaged that the boundaries among the three major blocks identified by morphotectonic analysis consist of long-lived, deep basement structures extending beneath the allochthonous tectonic units located in the hanging wall of the main thrust fault that controls the mountain front in the region. Such transversal basement structures interact with extensional seismogenic faults at hypocentral depths, thus playing a major role in the seismotectonic behavior of the study area. The UMAF are clearly segmented and traversed by crustal-scale faults. These faults may be seismogenic and responsible for large, deadly earthquakes that have been historically difficult to attribute to known, emergent faults.

The fact that the more uplifted area extends well beyond the footwall blocks of active normal faults is consistent with the relief pattern being the result of regional tectonic processes occurring on a much larger scale with respect to footwall uplift. This large-scale pattern of relief evolution

has been interpreted in terms of deep geodynamic processes affecting the segmented subducting slab (e.g., Faccenna et al., 2014; Menichelli et al., 2023). Indeed, most of the recent literature is all about dynamic support of the Apennines, with too little attention afforded to crustal-scale processes including active extension and shortening. Although the two types of 'deep' vs. 'shallow' processes are not mutually exclusive, the crustal structures discussed in this study suggest that the uplift pattern of the UMAF is mostly the result of lithosphere deformation – and particularly along-strike variations of crustal shortening mostly inherited from Late Miocene to Pliocene times – rather than dynamic support.

Our results, besides challenging the prevailing paradigm for recent Apennines uplift and surface strain by providing new insights into crustal-scale, along-strike segmentation of the belt (including the axial zone and the extensional system active there), may contribute to a better understanding of the complex tectonic behavior of active mountain belts in the Mediterranean region and elsewhere.

Supplementary data to this article can be found online at https://doi.org/10.1016/j.tecto.2024.230527.

CRediT authorship contribution statement

S. Teloni: Writing – original draft, Formal analysis, Data curation. **E. Valente:** Writing – original draft, Validation, Methodology, Conceptualization. **A. Ascione:** Writing – original draft, Validation, Methodology, Conceptualization. **S. Mazzoli:** Writing – original draft, Validation, Supervision, Conceptualization. **P.P. Pierantoni:** Visualization, Formal analysis. **M.C. Invernizzi:** Writing – original draft, Visualization, Supervision.

Declaration of competing interest

The authors declare that they have no known competing financial interests or personal relationships that could have appeared to influence the work reported in this paper.

Data availability

Data about the instrumental seismicity since 1985 derive from the Italian Seismological Instrumental and Parametric Data-Base (http://terremoti.ingv.it/iside ISIDe -INGV) and from the re-localized earthquakes by INGV Ancona (Cattaneo et al., 2017). Data about historical earthquakes with $M > 5.0$ derive by the Parametric Catalog of Italian Earthquakes – CPTI15-DBMI15 (Rovida et al., 2022). The 30 m NASA ASTER GDEM V2 (https://asterweb.jpl.nasa.gov/gdem.asp, last access on 8 December 2023) has been used for morphotectonic analysis. Maps have been created using Arcgis © (https://www.esri.com/it-it/arcgis/products/arcgis-online/overview), Matlab (https://it.mathworks.com/products/matlab.html) and CorelDraw (https://www.coreldraw.com/it/product/coreldraw/?topNav=it).

Acknowledgment

This paper is part of the Ph.D. thesis of Simone Teloni at the University of Camerino (Supervisor Prof. Chiara Invernizzi). We are grateful to the Editor (Prof. Gideon Rosenbaum) and two reviewers (Prof. Frank Pazzaglia and Dr. Dario Gioia) for their useful comments that helped us to improve the manuscript.

References

Ascione, A., Cinque, A., 1999. Tectonics and erosion in the long-term relief history of Southern Apennines (Italy). Zeitsch. Geomorphol. Suppl.-Bd. 117, 1–15.

Ascione, A., Cinque, A., Miccadei, E., Villani, F., Berti, C., 2008. The Plio-Quaternary uplift of the Apennines Chain: new data from the analysis of topography and river valleys in Central Italy. Geomorphology 102, 105–118. https://doi.org/10.1016/j.geomorph.2007.07.022.

Ascione, A., Ciarcia, S., Di Donato, V., Mazzoli, S., Vitale, S., 2012. The Pliocene-Quaternary wedge-top basins of southern Italy: an expression of propagating lateral slab tear beneath the Apennines. Basin Res. 24 (4), 456–474. https://doi.org/10.1111/j.1365-2117.2011.00534.x.

Barchi, M., Minelli, G., Pialli, G., 1998. The CROP 03 profile: a synthesis of results on deep structures of the Northern Apennines. Mem. Soc. Geol. Ital. 52, 383–400.

Barchi, M.R., Mirabella, F., 2009. The 1997–98 Umbria–Marche earthquake sequence: "Geological" vs. "seismological" faults. Tectonophysics 476 (1–2), 170–179. https://doi.org/10.1016/j.tecto.2008.09.013.

Barchi, M.R., Alvarez, W., Shimabukuro, D.H., 2012. The Umbria-Marche Apennines as a double orogen: observations and hypotheses. Ital. J. Geosci. 131 (2), 258–271. https://doi.org/10.3301/IJG.2012.17.

Basili, R., Barba, S., 2007. Migration and shortening rates in the northern Apennines, Italy: Implications for seismic hazard. Terra Nova 19 (6), 462–468. https://doi.org/10.1111/j.1365-3121.2007.00772.x.

Basilici, M., Ascione, A., Megna, A., Santini, S., Tavani, S., Valente, E., Mazzoli, S., 2020. Active deformation and relief evolution in the western Lurestan region of the Zagros mountain belt: new insights from tectonic geomorphology analysis and finite element modeling. Tectonics 39 (12), e2020TC006402. https://doi.org/10.1029/2020TC006402.

Bernard, T., Sinclair, H.D., Gailleton, B., Mudd, S.M., Ford, M., 2019. Lithological control on the post-orogenic topography and erosion history of the Pyrenees. Earth Planet. Sci. Lett. 518, 53–66. https://doi.org/10.1016/j.epsl.2019.04.034.

Bigi, S., Cantalamessa, G., Centamore, E., Didaskalou, P., Micarelli, A., Nisio, S., Pennesi, T., Potetti, M., 1997. The periadriatic basin (Marche-Abruzzi sector, Central Italy) during the Plio-Pleistocene. Giorn. Geol. 59 (1–2), 245–259.

Bishop, P., 2007. Long-term landscape evolution: linking tectonics and surface processes. Earth Surf. Process. Landf. 32 (3), 329–365. https://doi.org/10.1002/esp.1493.

Bitonte, R., Livio, F.A., Mazzoli, S., Bellentani, G., Di Cesare, L., Dall'Igna, M., Castelluccio, A., Scaramuzzo, E., 2021. Frontal accretion vs. foreland plate deformation: discriminating the style of post-collisional shortening in the Apennines. J. Struct. Geol. 145, 104290. https://doi.org/10.1016/j.jsg.2021.104290.

Brogi, A., Capezzuoli, E., Martini, I., Picozzi, M., Sandrelli, F., 2014. Late Quaternary tectonics in the inner Northern Apennines (Siena Basin, southern Tuscany, Italy) and their seismotectonic implication. J. Geodyn. 76, 25–45. https://doi.org/10.1016/j.jog.2014.03.001.

Bull, W.B., 2008. Tectonic Geomorphology of Mountains: A New Approach to Paleoseismology. John Wiley & Sons. https://doi.org/10.1002/9780470692318.

Bull, W.B., McFadden, L.D., 1977. Tectonic Geomorphology North and South of the Garlock Fault, California. In: Doehring, D.O. (Ed.), Geomorphology in Arid Regions: A Proceedings Volume of the 8th Annual Geomorphology Symposium. State University of New York, Binghamton, NY, pp. 115–138. https://doi.org/10.4324/9780429299230-5.

Burbank, D.W., Anderson, R.S., 2011. Tectonic Geomorphology. John Wiley & Sons, Chichester, United Kingdom. https://doi.org/10.1002/9781444345063.

Buscher, J.T., Ascione, A., Valente, E., 2017. Decoding the role of tectonics, incision and lithology on drainage divide migration in the Mt. Alpi region, southern Apennines, Italy. Geomorphology 276, 37–50. https://doi.org/10.1016/j.geomorph.2016.10.003.

Butler, R.W.H., Mazzoli, S., Corrado, S., De Donatis, M., Di Bucci, D., Gambini, R., Naso, G., Nicolai, C., Scrocca, D., Shiner, P., Zucconi, V., 2004. Applying thick-skinned tectonic models to the Apennine thrust belt of Italy— Limitations and implications. In: McClay, K.R. (Ed.), Thrust Tectonics and Hydrocarbon Systems: AAPG Memoir, vol. 82, pp. 647–667. https://doi.org/10.1306/M82813C34.

Calamita, F., Pizzi, A., 1994. Recent and active extensional tectonics in the southern Umbro-Marchean Apennines (Central Italy). Mem. Soc. Geol. Ital. 48, 541–548.

Calamita, F., Deiana, G., Invernizzi, C., Pizzi, A., 1991. Tettonica. In: Marche Assessorato urbanistica e ambiente (Ed.), L'ambiente fisico delle Marche: geologia, geomorfologia e idrogeologia (69–80). Ed. Selca, Firenze, Italy.

Calamita, F., Cello, G., Deiana, G., Paltrinieri, W., 1994. Structural styles, chronology rates of deformation, and time-space relationships in the Umbria-Marche thrust system (central Apennines, Italy). Tectonics 13 (4), 873–881. https://doi.org/10.1029/94TC00276.

Calderoni, G., Della Seta, M., Fredi, P., Lupia Palmieri, E., Nesci, O., Savelli, D., Troiani, F., 2010. Late Quaternary Geomorphological Evolution of the Adriatic Coast Reach Encompassing the Metauro, Cesano and Misa River Mouths (Northern Marche, Italy), 3. Geo Acta Special Publication, pp. 109–124.

Cantalamessa, G., Di Celma, C., 2004. Sequence response to syndepositional regional uplift: insights from high-resolution sequence stratigraphy of late early Pleistocene strata, Periadriatic Basin, Central Italy. Sediment. Geol. 164 (3–4), 283–309. https://doi.org/10.1016/j.sedgeo.2003.11.003.

Cantalamessa, G., Centamore, E., Chiocchini, U., Colalongo, M.L., Micarelli, A., Nanni, T., Pasini, G., Potetti, M., Ricci Lucchi, F., 1986. Il Plio-Pleistocene delle Marche. Studi Geol. Camerti 61–81.

Castelli, V., Monachesi, G., 2001. Seismic history and historical earthquake scenario for the town of Fabriano (Central Italy). Italian Geotech. J. 35 (2), 36–46.

Cattaneo, M., Frapiccini, M., Ladina, C., Marzorati, S., Monachesi, G., 2017. A mixed automatic-manual seismic catalog for Central-Eastern Italy: Analysis of homogeneity. Ann. Geophys. 60 (6). https://doi.org/10.4401/AG-7333.

Centamore, E., Nisio, S., 2003. Effects of uplift and tilting in the Central-Northern Apennines (Italy). Quat. Int. 101, 93–101. https://doi.org/10.1016/S1040-6182(02)00092-7.

Centamore, E., Rossi, D., 2009. Neogene-Quaternary tectonics and sedimentation in the Central Apennines. Ital. J. Geosci. 128 (1), 73–88. https://doi.org/10.3301/ijg.2009.128.1.73.

Centamore, E., Fumanti, F., Nisio, S., 2002. The central-northern Apennines geological evolution from Triassic to Neogene time. Boll. Soc. Geol. Ital. Spec. 1, 181–197.
Chiaraluce, L., Amato, A., Cocco, M., Chiarabba, C., Selvaggi, G., Di Bona, M., Ripepe, M., 2004. Complex normal faulting in the Apennines thrust-and-fold belt: the 1997 seismic sequence in Central Italy. Bull. Seismol. Soc. Am. 94 (1), 99–116. https://doi.org/10.1785/0120020052.
Cinque, A., Patacca, E., Scandone, P., Tozzi, M., 1993. Quaternary Kinematic Evolution of the Southern Appennines. Relationships Between Surface Geological Features and Deep Lithospheric Structures. https://doi.org/10.4401/ag-4283.
Cipollari, P., Cosentino, D., Gliozzi, E., 1999. Extension and compression related basins in Central Italy during the Messinian Lago-Mare event. Tectonophysics 315 (1–4), 163–185. https://doi.org/10.1016/S0040-1951(99)00287-5.
Civico, R., Pucci, S., Villani, F., Pizzimenti, L., de Martini, P.M., Nappi, R., EMERGEO Working Group, 2018. Surface ruptures following the 30 October 2016 Mw 6.5 Norcia earthquake, Central Italy. J. Maps 14 (2). https://doi.org/10.1080/17445647.2018.1441756.
Clementucci, R., Ballato, P., Siame, L.L., Faccenna, C., Yaaqoub, A., Essaifi, A., Leanni, L., Guillou, V., 2022. Lithological control on topographic relief evolution in a slow tectonic setting (Anti-Atlas, Morocco). Earth Planet. Sci. Lett. 596, 117788. https://doi.org/10.1016/j.epsl.2022.117788.
Conti, P., Cornamusini, G., Carmignani, L., 2020. An outline of the geology of the Northern Apennines (Italy), with geological map at 1: 250,000 scale. Ital. J. Geosci. 139 (2), 149–194. https://doi.org/10.3301/IJG.2019.25.
Cornamusini, G., Conti, P., Bonciani, F., Callegari, I., Martelli, L., 2017. Geology of the 'Coltre della Val Marecchia' (Romagna-Marche Northern Apennines, Italy). J. Maps 13 (2), 207–218. https://doi.org/10.1080/17445647.2017.1290555.
Cosentino, D., Asti, R., Nocentini, M., Gliozzi, E., Kotsakis, T., Mattei, M., Esu, D., Spadi, M., Tallini, M., Cifelli, F., Pennacchioni, M., Cavuoto, G., Di Fiore, V., 2017. New insights into the onset and evolution of the central Apennine extensional intermontane basins based on the tectonically active L'Aquila Basin (Central Italy). GSA Bull. 129 (9–10), 1314–1336. https://doi.org/10.1130/B31679.1.
Costa, M., Chicco, J., Invernizzi, C., Teloni, S., Pierantoni, P.P., 2021. Plio–Quaternary structural evolution of the outer sector of the Marche Apennines South of the Conero Promontory, Italy. Geosciences 11 (5), 184. https://doi.org/10.3390/geosciences11050184.
Costa, M., Invernizzi, C., Penza, G., Teloni, S., Pierantoni, P.P., 2023. Seismotectonic role of transversal structures in the Plio-Quaternary evolution of the external Marche Apennines (Italy). J. Geol. Soc. Lond. 180 (6). https://doi.org/10.1144/jgs2023-002 jgs2023-002.
Coward, M.P., De Donatis, M., Mazzoli, S., Paltrinieri, W., Wezel, F.C., 1999. Frontal part of the northern Apennines fold and thrust belt in the Romagna-Marche area (Italy): Shallow and deep structural styles. Tectonics 18 (3), 559–574. https://doi.org/10.1029/1999TC900003.
D'Agostino, N., Jackson, J.A., Dramis, F., Funiciello, R., 2001. Interactions between mantle upwelling, drainage evolution and active normal faulting: an example from the central Apennines (Italy). Geophys. J. Int. 147 (2), 475–497. https://doi.org/10.1046/j.1365-246X.2001.00539.x.
Dahlstrom, C.D., 1970. Structural geology in the eastern margin of the Canadian Rocky Mountains. Bull. Can. Petrol. Geol. 18 (3), 332–406. https://doi.org/10.35767/gscpgbull.18.3.332.
D'Alessandro, L., Miccadei, E., Piacentini, T., 2003. Morphostructural elements of Central–Eastern Abruzzi: contributions to the study of the role of tectonics on the morphogenesis of the Apennine chain. Quat. Int. 101, 115–124. https://doi.org/10.1016/S1040-6182(02)00094-0.
Das, S., Kandekar, A.M., Sangode, S.J., 2022. Lithologic control on geomorphic evolution of the Central Western Gaths: an example from the Aghnashini catchment, Karnataka, India. J. Geol. Soc. India 98, 451–459. https://doi.org/10.1007/s12594-022-2001-6.
Deiana, G., Cello, G., Chiocchini, M., Galdenzi, S., Mazzoli, S., Pistolesi, E., Potetti, M., Romano, A., Turco, E., Principi, M., 2002. Tectonic evolution of the external zones of the Umbria-Marche Apennines in the Monte San Vicino-Cingoli area. Boll. Della Soc. Geol. Ital. 121 (1), 229–238.
Deiana, G., Mazzoli, S., Paltrinieri, W., Pierantoni, P.P., Romano, A., 2003. Struttura del fronte montuoso umbro-marchigiano-sabino. Studi Geol. Camerti Spec. 2003, 15–36.
Delchiaro, M., Iacobucci, G., Della Seta, M., Gribenski, N., Piacentini, D., Ruscitto, V., Troiani, F., 2024. A fluvial record of late Quaternary climate changes and tectonic uplift along the Marche Piedmont Zone of the Apennines: new insights from the Tesino River (Italy). Geomorphology 445, 108971. https://doi.org/10.1016/j.geomorph.2023.108971.
Della Seta, M., Del Monte, M., Fredi, P., Miccadei, E., Nesci, O., Pambianchi, G., Piacentini, T., Troiani, F., 2008. Morphotectonic evolution of the Adriatic piedmont of the Apennines: an advancement in the knowledge of the Marche-Abruzzo border area. Geomorphology 102 (1), 119–129. https://doi.org/10.1016/j.geomorph.2007.06.018.
Dewey, J.F., 1988. Extensional collapse of orogens. Tectonics 7 (6), 1123–1139. https://doi.org/10.1029/TC007i006p01123.
Dewey, J.F., Helman, M.L., Knott, S.D., Turco, E., Hutton, D.H.W., 1989. Kinematics of the western Mediterranean. Geol. Soc. Lond. Spec. Publ. 45 (1), 265–283. https://doi.org/10.1144/GSL.SP.1989.045.01.15.
Di Biase, R.A., Whipple, K.X., Heimsath, A.M., Ouimet, W.B., 2010. Landscape form and millennial erosion rates in the San Gabriel Mountains, CA. Earth Planet. Sci. Lett. 289 (1–2), 134–144. https://doi.org/10.1016/j.epsl.2009.10.036.
Doglioni, C., 1995. Geological remarks on the relationships between extension and convergent geodynamic settings. Tectonophysics 252 (1–4), 253–267. https://doi.org/10.1016/0040-1951(95)00087-9.
Doglioni, C., Dagostino, N., Mariotti, G., 1998. Normal faulting vs regional subsidence and sedimentation rate. Mar. Pet. Geol. 15 (8), 737–750. https://doi.org/10.1016/S0264-8172(98)00052-X.
Duvall, A., Kirby, E., Burbank, D., 2004. Tectonic and lithologic controls on bedrock channel profiles and processes in coastal California. J. Geophys. Res. Earth 109 (F3). https://doi.org/10.1029/2003jf000086.
Eizenhöfer, P.R., McQuarrie, N., Shelef, E., Ehlers, T.A., 2019. Landscape response to lateral advection in convergent orogens over geologic time scales. J. Geophys. Res. Earth 124, 2056–2078. https://doi.org/10.1029/2019JF005100.
EMERGEO Working Group, 2016. Coseismic effects of the 2016 Amatrice seismic sequence: first geological results. Ann. Geophys. Italy 59 (5). https://doi.org/10.4401/ag-7195.
England, P., Molnar, P., 1990. Surface uplift, uplift of rocks, and exhumation of rocks. Geology 18 (12), 1173–1177. https://doi.org/10.1130/0091-7613(1990)018<1173:SUUORA>2.3.CO;2.
Erlanger, E.D., Rugenstein, J.K.C., Bufe, A., Picotti, V., Willett, S.D., 2021. Controls on physical and chemical denudation in a mixed carbonate-siliciclastic orogen. J. Geophys. Res. Earth 126 (8). https://doi.org/10.1029/2021JF006064 e2021JF006064.
Faccenna, C., Becker, T.W., Miller, M.S., Serpelloni, E., Willett, S.D., 2014. Isostasy, dynamic topography, and the elevation of the Apennines of Italy. Earth Planet. Sci. Lett. 407, 163–174. https://doi.org/10.1016/j.epsl.2014.09.027.
Fadul, C.M., Oliveira, P., Val, P., 2022. Ongoing landscape transience in the eastern Amazon Craton consistent with lithologic control of base level. Earth Surf. Process. Landf. 47, 3117–3132. https://doi.org/10.1002/esp.5447.
Fellin, M.G., San Jose, M., Faccenna, C., Willett, S.D., Cosentino, D., Lanari, R., Maden, C., 2022. Transition from slab roll-back to slab break-off in the central Apennines, Italy: Constraints from the stratigraphic and thermochronologic record. GSA Bull. 134 (7–8), 1916–1930. https://doi.org/10.1130/B36123.1.
Ferrarini, F., Arrowsmith, J.R., Brozzetti, F., de Nardis, R., Cirillo, D., Whipple, K.X., Cheng, F., 2021. Late quaternary tectonics along the peri-adriatic sector of the Apenninic Chain (Central-Southern Italy): inspecting active shortening through topographic relief and fluvial network analyses. Lithosphere 2021 (1). https://doi.org/10.2113/2021/7866617.
Forte, A.M., Cowgill, E., Whipple, K.X., 2014. Transition from a singly vergent to doubly vergent wedge in a young orogen: the Greater Caucasus. Tectonics 33 (11), 2077–2101. https://doi.org/10.1002/2014TC003651.
Frepoli, A., Amato, A., 1997. Contemporaneous extension and compression in the Northern Apennines from earthquake fault-plane solutions. Geophys. J. Int. 129 (2), 368–388. https://doi.org/10.1111/j.1365-246X.1997.tb01589.x.
Galadini, F., Messina, P., 2001. Plio-Quaternary changes of the normal fault architecture in the central Apennines (Italy). Geodin. Acta 14 (6), 321–344. https://doi.org/10.1080/09853111.2001.10510727.
Gallen, S.F., Wegmann, K.W., 2017. River profile response to normal fault growth and linkage: an example from the Hellenic forearc of south-Central Crete, Greece. Earth Surf. Dynam. 5 (1), 161–186. https://doi.org/10.5194/esurf-5-161-2017.
Gentili, B., Pambianchi, G., Aringoli, D., Materazzi, M., Giacopetti, M., 2017. Pliocene-Pleistocene geomorphological evolution of the Adriatic side of Central Italy. Geol. Carpath. 68 (1), 6. https://doi.org/10.1515/geoca-2017-0001.
Guerra, V., Lazzari, M., 2020. Geomorphic approaches to estimate shortterm erosion rates: An example from Valmarecchia River system (Northern Apennines, Italy). Water (Basel) 12, 2535. https://doi.org/10.3390/w12092535.
ISIDe Working Group, 2007. Italian Seismological Instrumental and Parametric Database (ISIDe). Istituto Nazionale di Geofisica e Vulcanologia (INGV). https://doi.org/10.13127/ISIDE
Jaiswara, N.K., Kotluri, S.K., Pandey, P., Pandey, A.K., 2020. MATLAB functions for extracting hypsometry, stream-length gradient index, steepness index, chi gradient of channel and swath profiles from digital elevation model (DEM) and other spatial data for landscape characterization. Appl. Comp. Geosci. 7, 100033. https://doi.org/10.1016/j.acags.2020.100033.
Keller, A.E., Pinter, N., 2002. Active Tectonics and Earthquakes, Uplift, and Landscape, 2nd ed. Prentice Hall, London, United Kingdom.
Keller, J.V.A., Minelli, G., Pialli, G., 1994. Anatomy of late orogenic extension: the Northern Apennines case. Tectonophysics 238 (1–4), 275–294. https://doi.org/10.1016/0040-1951(94)90060-4.
Kirby, E., Whipple, K., 2001. Quantifying differential rock-uplift rates via stream profile analysis. Geology 29 (5), 415–418. https://doi.org/10.1130/0091-7613(2001)029<0415:QDRURV>2.0.CO;2.
Lanari, R., Reitano, R., Giachetta, E., Pazzaglia, F.J., Clementucci, R., Faccenna, C., Fellin, M.G., 2022. Is the Anti-Atlas of Morocco still uplifting? J. Afr. Earth Sci. 188, 104481. https://doi.org/10.1016/j.jafrearsci.2022.104481.
Lanari, R., Reitano, R., Faccenna, C., Agostinetti, N.P., Ballato, P., 2023. Surface and crustal response to deep subduction dynamics: insights from the Apennines, Italy. Tectonics 42 (3). https://doi.org/10.1029/2022TC007461 e2022TC007461.
Lucente, F.P., Chiarabba, C., Cimini, G.B., Giardini, D., 1999. Tomographic constraints on the geodynamic evolution of the Italian region. J. Geophys. Res. Solid Earth 104 (B9), 20307–20327. https://doi.org/10.1029/1999JB900147.
Mancini, M., Cavinato, G.P., Blum, M., Marriot, S., Leclair, S., 2005. The Middle Valley of the Tiber River, Central Italy: Plio-Pleistocene Fluvial and Coastal Sedimentation, Extensional Tectonics and Volcanism, 35. Fluvial Sedimentology VII. IAS Spec. Publ, pp. 373–396. https://doi.org/10.1002/9781444304350.ch20.
Martini, I.P., Sagri, M., 1993. Tecto-sedimentary characteristics of late Miocene-Quaternary extensional basins of the Northern Apennines, Italy. Earth Sci. Rev. 34 (3), 197–233. https://doi.org/10.1016/0012-8252(93)90034-5.
Materazzi, M., Bufalini, M., Dramis, F., Pambianchi, G., Gentili, B., Di Leo, M., 2022. Active tectonics and paleoseismicity of a transverse lineament in the Fabriano valley,

Umbria-Marche Apennine (Central Italy). Int. J. Earth Sci. 111, 1539–1549. https://doi.org/10.1007/s00531-022-02198-x.
Mayer, L., Menichetti, M., Nesci, O., Savelli, D., 2003. Morphotectonic approach to the drainage analysis in the North Marche region, Central Italy. Quat. Int. 101, 157–167. https://doi.org/10.1016/S1040-6182(02)00098-8.
Mazzoli, S., Helman, M., 1994. Neogene patterns of relative plate motion for Africa-Europe: some implications for recent Central Mediterranean tectonics. Geol. Rundsch. 83, 464–468. https://doi.org/10.1007/BF00210558.
Mazzoli, S., Pierantoni, P.P., Borraccini, F., Paltrinieri, W., Deiana, G., 2005. Geometry, segmentation pattern and displacement variations along a major Apennine thrust zone, Central Italy. J. Struct. Geol. 27 (11), 1940–1953. https://doi.org/10.1016/j.jsg.2005.06.002.
Mazzoli, S., Macchiavelli, C., Ascione, A., 2014. The 2013 Marche offshore earthquakes: new insights into the active tectonic setting of the outer northern Apennines. J. Geol. Soc. Lond. 171 (4), 457–460. https://doi.org/10.1144/jgs2013-091.
Mazzoli, S., Santini, S., Macchiavelli, C., Ascione, A., 2015. Active tectonics of the outer northern Apennines: Adriatic vs. Po Plain seismicity and stress fields. J. Geodyn. 84, 62–76. https://doi.org/10.1016/j.jog.2014.10.002.
Mele, G., Rovelli, A., Seber, D., Hearn, T.M., Barazangi, M., 1998. Compressional velocity structure and anisotropy in the uppermost mantle beneath Italy and surrounding regions. J. Geophys. Res. Solid Earth 103 (B6), 12529–12543. https://doi.org/10.1029/98JB00596.
Miccadei, E., Piacentini, T., Buccolini, M., 2017. Long-term geomorphological evolution in the Abruzzo area, Central Italy: twenty years of research. Geol. Carpath. 68 (1), 19. https://doi.org/10.1515/geoca-2017-0002.
Monachesi, G., Castelli, V., Vasapollo, N., 1991. Historical earthquakes in Central Italy: case histories in the Marche area. Tectonophysics 193 (1–3), 95–107. https://doi.org/10.1016/0040-1951(91)90191-T.
Montuori, C., Cimini, G.B., Favali, P., 2007. Teleseismic tomography of the southern Tyrrhenian subduction zone: New results from seafloor and land recordings. J. Geophys. Res. Solid Earth 112 (B3). https://doi.org/10.1029/2005JB004114.
Nesci, O., Savelli, D., 2003. Diverging drainage in the Marche Apennines (Central Italy). Quat. Int. 101, 203–209. https://doi.org/10.1016/S1040-6182(02)00102-7.
Nesci, O., Savelli, D., Troiani, F., 2012. Types and development of stream terraces in the Marche Apennines (Central Italy): a review and remarks on recent appraisals. Géomorphol.: Relief, Proc. Environ. 18 (2), 215–238. https://doi.org/10.4000/geomorphologie.9838.
Obaid, A.K., Allen, M.B., 2019. Landscape expressions of tectonics in the Zagros fold-and-thrust belt. Tectonophysics 766, 20–30. https://doi.org/10.1016/j.tecto.2019.05.024.
Ori, G.G., Serafini, G., Visentin, C., Ricci Lucchi, F., Casnedi, R., Colalongo, M.L., Mosna, S., 1991. The Pliocene-Pleistocene Adriatic Foredeep (Marche and Abruzzo, Italy): An integrated approach to surface and subsurface geology. In: 3rd EAPG Conference, Adriatic Foredeep Field Trip Guide Book. EAPG and AGIP, Florence, Italy, pp. 26–30.
Ott, R.F., Gallen, S.F., Caves Rugenstein, J.K., Ivy-Ochs, S., Helman, D., Fassoulas, C., Willett, S.D., 2019. Chemical versus mechanical denudation in meta-clastic and carbonate bedrock catchments on Crete, Greece, and mechanisms for steep and high carbonate topography. J. Geophys. Res. Earth 124 (12), 2943–2961. https://doi.org/10.1029/2019JF005142.
Pace, P., Scisciani, V., Calamita, F., Butler, R.W., Iacopini, D., Esestime, P., Hodgson, N., 2015. Inversion structures in a foreland domain: seismic examples from the Italian Adriatic Sea. Interpretation 3 (4). https://doi.org/10.1190/INT-2015-0013.1. SAA161-SAA176.
Pascucci, V., Martini, I.P., Sagri, M., Sandrelli, F., Nichols, G., 2007. Effects of transverse structural lineaments on the Neogene-Quaternary basins of Tuscany (inner Northern Apennines, Italy). Sediment. Process. Environ. Basins 38, 155–182. https://doi.org/10.1002/9781444304411.ch8.
Patacca, E., Sartori, R., Scandone, P., 1990. Tyrrhenian basin and Apenninic arcs: kinematic relations since late Tortonian times. Mem. Soc. Geol. Ital. 45, 425–451.
Pazzaglia, F.J., Fisher, J.A., 2022. A reconstruction of Apennine uplift history and the development of transverse drainages from longitudinal profile inversion. In: In from the Guajira Desert to the Apennines, and from Mediterranean Microplates to the Mexican Killer Asteroid: Honoring the Career of Walter Alvarez. Geological Society of America. https://doi.org/10.1130/2022.2557(09).
Pazzaglia, F.J., Gardner, T.W., Merritts, D.J., 1998. Bedrock fluvial incision and longitudinal profile development over geologic time scales determined by fluvial terraces. Geophys. Monogr.-Am. Geophys. Union 107, 207–236. https://doi.org/10.1029/GM107p0207.
Pérez-Peña, J.V., Al-Awabdeh, M., Azañón, J.M., Galve, J.P., Booth-Rea, G., Notti, D., 2017. SwathProfiler and NProfiler: two new ArcGIS Add-ins for the automatic extraction of swath and normalized river profiles. Comput. Geosci. 104, 135–150. https://doi.org/10.1016/j.cageo.2016.08.008.
Perron, J.T., Royden, L., 2013. An integral approach to bedrock river profile analysis. Earth Surf. Process. Landf. 38 (6), 570–576. https://doi.org/10.1002/esp.3302.
Pezzo, G., Billi, A., Carminati, E., Conti, A., De Gori, P., Devoti, R., Lucente, F.P., Palano, M., Petracchini, L., Serpelloni, E., Tavani, S., Chiarabba, C., 2023. Seismic source identification of the 9 November 2022 Mw 5.5 offshore Adriatic Sea (Italy) earthquake from GNSS data and aftershock relocation. Sci. Rep. 13, 11474. https://doi.org/10.1038/s41598-023-38150-5.
Piacentini, T., Miccadei, E., 2014. The role of drainage systems and intermontane basins in the Quaternary landscape of the Central Apennines chain (Italy). Rendic. Lincei 25, 139–150. https://doi.org/10.1007/s12210-014-0312-2.
Pierantoni, P.P., Deiana, G., Galdenzi, S., 2013. Stratigraphic and structural features of the Sibillini mountains (Umbria-Marche Apennines, Italy). Ital. J. Geosci. 132 (3), 497–520. https://doi.org/10.3301/IJG.2013.08.
Pierantoni, P.P., Chicco, J., Costa, M., Invernizzi, C., 2019. Plio-Quaternary transpressive tectonics: a key factor in the structural evolution of the outer Apennine–Adriatic system, Italy. J. Geol. Soc. 176 (6), 1273–1283. https://doi.org/10.1144/jgs2018-199.
Piromallo, C., Morelli, A., 2003. P wave tomography of the mantle under the Alpine-Mediterranean area. J. Geophys. Res. Solid Earth 108 (B2). https://doi.org/10.1029/2002JB001757.
Racano, S., Fubelli, G., Ernesto, C., Bonasera, M., Francesco, D., 2020. Geomorphological detection of surface effects induced by active blind thrusts in the southern Abruzzi peri-Adriatic belt (Central Italy). Geogr. Fis. Din. Quat. 43, 3–13. https://doi.org/10.4461/GFDQ.2020.43.1.
Racano, S., Schildgen, T.F., Cosentino, D., Miller, S.R., 2021. Temporal and Spatial Variations in Rock Uplift from River-Profile Inversions at the Central Anatolian Plateau Southern margin. J. Geophys. Res. Earth 126. https://doi.org/10.1029/2020JF006027 e2020JF006027.
Racano, S., Van der Beek, P.A., Schildgen, T.F., Faccenna, C., Buleo Tebar, V., Cosentino, D., 2024. Slab driven Quaternary rock-uplift and topographic evolution in the northern-central Apennines from linear inversion of the drainage system. Geochem. Geophys. Geosyst. 25. https://doi.org/10.1029/2024GC011592 e2024GC011592.
Ricci Lucchi, F., 1986. The Oligocene to recent foreland basins of the northern Apennines. In: Foreland Basins, vol. 8. Blackwell Scientific Oxford, pp. 105–139.
Rovida, A., Locati, M., Camassi, R., Lolli, B., Gasperini, P., Antonucci, A., 2022. Catalogo Parametrico dei Terremoti Italiani CPTI15, versione 4.0. https://doi.org/10.13127/cpti/cpti15.4.
Royden, L., Perron, T.J., 2013. Solutions of the stream power equation and application to the evolution of river longitudinal profiles. J. Geophys. Res. Earth 118 (2), 497–518. https://doi.org/10.1002/jgrf.20031.
San Jose, M., Rugenstein, J.K.C., Cosentino, D., Faccenna, C., Fellin, M.G., Ghinassi, M., Martini, I., 2020. Stable isotope evidence for rapid uplift of the central Apennines since the late Pliocene. Earth Planet. Sci. Lett. 544, 116376. https://doi.org/10.1016/j.epsl.2020.116376.
Santini, S., Saggese, F., Megna, A., Mazzoli, S., 2011. A note on Central-Northern Marche seismicity: new focal mechanisms for events recorded in years 2003-2009. Boll. Geofis. Teor. Appl. 52 (4). https://doi.org/10.4430/bgta0025.
Santini, S., Mazzoli, S., Megna, A., Candela, S., 2016. Thermal Structure of the Outer Northern Apennines along the CROP-03 Profile. J. Geogr. Geol. 8 (4). https://doi.org/10.5539/jgg.v8n4p1.
Santini, S., Basilici, M., Invernizzi, C., Jablonska, D., Mazzoli, S., Megna, A., Pierantoni, P.P., 2021. Controls of Radiogenic Heat and Moho Geometry on the thermal setting of the Marche Region (Central Italy): an Analytical 3D Geothermal Model. Energies 14, 6511. https://doi.org/10.3390/en14206511.
Schildgen, T.F., Cosentino, D., Caruso, A., Buchwaldt, R., Yıldırım, C., Bowring, S.A., Rojay, B., Echtler, H., Strecker, M.R., 2012. Surface expression of eastern Mediterranean slab dynamics: Neogene topographic and structural evolution of the southwest margin of the Central Anatolian Plateau, Turkey. Tectonics 31 (2). https://doi.org/10.1029/2011TC003021.
Schwanghart, W., Kuhn, N.J., 2010. TopoToolbox: A set of Matlab functions for topographic analysis. Environ. Model Softw. 25 (6), 770–781. https://doi.org/10.1016/j.envsoft.2009.12.002.
Schwanghart, W., Scherler, D., 2014. TopoToolbox 2–MATLAB-based software for topographic analysis and modeling in Earth surface sciences. Earth Surf. Dyn. 2 (1), 1–7. https://doi.org/10.5194/esurf-2-1-2014.
Scisciani, V., Agostini, S., Calamita, F., Pace, P., Cilli, A., Giori, I., Paltrinieri, W., 2014. Positive inversion tectonics in foreland fold-and-thrust belts: a reappraisal of the Umbria–Marche Northern Apennines (Central Italy) by integrating geological and geophysical data. Tectonophysics 637, 218–237. https://doi.org/10.1016/j.tecto.2014.10.010.
Scotti, V.N., Molin, P., Faccenna, C., Soligo, M., Casas-Sainz, A., 2014. The influence of surface and tectonic processes on landscape evolution of the Iberian Chain (Spain): quantitative geomorphological analysis and geochronology. Geomorphology 206, 37–57. https://doi.org/10.1016/j.geomorph.2013.09.017.
Seagren, E.G., Schoenbohm, L.M., 2019. Base level and lithologic control of drainage reorganization in the Sierra de las Planchadas, NW Argentina. J. Geophys. Res.: EarthSurf. 124, 1516–1539. https://doi.org/10.1029/2018JF004885.
Sembroni, A., Molin, P., Soligo, M., Tuccimei, P., Anzalone, E., Billi, A., Franchini, S., Ranaldi, M., Tarchini, L., 2020. The uplift of the Adriatic flank of the Apennines since the Middle Pleistocene: New insights from the Tronto River basin and the Acquasanta Terme Travertine (Central Italy). Geomorphology 352, 106990. https://doi.org/10.1016/j.geomorph.2019.106990.
Serpelloni, E., Faccenna, C., Spada, G., Dong, D., Williams, S.D., 2013. Vertical GPS ground motion rates in the Euro-Mediterranean region: New evidence of velocity gradients at different spatial scales along the Nubia-Eurasia plate boundary. J. Geophys. Res. Solid Earth 118 (11), 6003–6024. https://doi.org/10.1002/2013JB010102.
Spakman, W., 1990. Tomographic images of the upper mantle below Central Europe and the Mediterranean. Terra Nova 2 (6), 542–553. https://doi.org/10.1111/j.1365-3121.1990.tb00119.
Spakman, W., Wortel, R., 2004. A tomographic view on western Mediterranean geodynamics. In: The TRANSMED Atlas. The Mediterranean Region from Crust to Mantle: Geological and Geophysical Framework of the Mediterranean and the Surrounding Areas (pp. 31-52). Springer Berlin Heidelberg, Berlin, Heidelberg. https://doi.org/10.1007/978-3-642-18919-7_2.
Stock, J.D., Montgomery, D.R., 1999. Geologic constraints on bedrock river incision using the stream power law. J. Geophys. Res. Solid Earth 104 (B3), 4983–4993. https://doi.org/10.1029/98JB02139.

Stucchi, M., Monachesi, G., Mandrelli, F.M., 1991. Investigation of 18th century seismicity in Central Italy in the light of the 1741 Fabriano earthquake. Tectonophysics 193 (1–3), 65–82. https://doi.org/10.1016/0040-1951(91)90189-Y.

Tavarnelli, E., Scisciani, V., Patruno, S., Calamita, F., Pace, P., Iacopini, D., 2019. The role of structural inheritance in the evolution of foldand-thrust belts: insights from the Umbria-Marche Apennines, Italy. In: Koeberl, C., Bice, D.M. (Eds.), 250 Million Years of Earth History in Central Italy: Celebrating 25 Years of the Geological Observatory of Coldigioco, 542. Geological Society of America, Special Paper, pp. 191–211. https://doi.org/10.1130/2019.2542(10).

Turco, E., Macchiavelli, C., Penza, G., Schettino, A., Pierantoni, P.P., 2021. Kinematics of deformable blocks: application to the opening of the tyrrhenian basin and the formation of the apennine Chain. Geosciences 11 (4), 177. https://doi.org/10.3390/geosciences11040177.

Valente, E., Buscher, J.T., Jourdan, F., Petrosino, P., Reddy, S.M., Tavani, S., Corradetti, A., Tavani, S., 2019. Constraining mountain front tectonic activity in extensional setting from geomorphology and Quaternary stratigraphy: a case study from the Matese ridge, southern Apennines. Quat. Sci. Rev. 219, 47–67. https://doi.org/10.1016/j.quascirev.2019.07.001.

Vannoli, P., Basili, R., Valensise, G., 2004. New geomorphic evidence for anticlinal growth driven by blind-thrust faulting along the northern Marche coastal belt (Central Italy). J. Seismol. 8, 297–312. https://doi.org/10.1023/B:JOSE.0000038456.00574.e3.

Vannoli, P., Vannucci, G., Bernardi, F., Palombo, B., Ferrari, G., 2015. The source of the 30 October 1930 M w 5.8 Senigallia (Central Italy) earthquake: A convergent solution from instrumental, macroseismic, and geological data. Bull. Seismol. Soc. Am. 105 (3), 1548–1561. https://doi.org/10.1785/0120140263.

Veneri, F., 1986. La colata gravitativa della Val Marecchia. In: Centamore, E., Deiana, G. (Eds.), La geologia delle Marche. Studi Geol. Camerti, volume speciale, Camerino, pp. 83–87.

Wegmann, K.W., Pazzaglia, F.J., 2009. Late Quaternary fluvial terraces of the Romagna and Marche Apennines, Italy: Climatic, lithologic, and tectonic controls on terrace genesis in an active orogen. Quat. Sci. Rev. 28 (1–2), 137–165. https://doi.org/10.1016/j.quascirev.2008.10.006.

Westaway, R., 1993. Quaternary uplift of southern Italy. J. Geophys. Res. Solid Earth 98 (B12), 21741–21772. https://doi.org/10.1029/93JB01566.

Whipple, K.X., Wobus, C., Crosby, B., Kirby, E., Sheehan, D., 2007. New Tools for Quantitative Geomorphology: Extraction and Interpretation of Stream Profiles from Digital Topographic Data. GSA short course, 506, Http://Geomorphtools.Org/Tools/StPro/Tutorials/StPro_UserGuidees_Final.Pdf.

Whittaker, A.C., Attal, M., Cowie, P.A., Tucker, G.E., Roberts, G., 2008. Decoding temporal and spatial patterns of fault uplift using transient river long profiles. Geomorphology 100 (3–4), 506–526. https://doi.org/10.1016/j.geomorph.2008.01.018.

Wiemer, S., 2001. A software package to analyze seismicity: ZMAP. Seismol. Res. Lett. 72 (3), 373–382. https://doi.org/10.1785/gssrl.72.3.373.

Wortel, M.J.R., Spakman, W., 2000. Subduction and slab detachment in the Mediterranean-Carpathian region. Science 290 (5498), 1910–1917. https://doi.org/10.1126/science.290.5498.1910.